DEVELOPMENT, VALIDATION, AND SENSITIVITY ANALYSES OF HUMAN EYE MOVEMENT MODELS*

Author: **A. Terry Bahill**
Biomedical Engineering Program
Department of Electrical Engineering
Carnegie-Mellon University and
Department of Neurology
University of Pittsburgh Medical School
Pittsburgh, Pennsylvania

Referee: Lawrence Stark
Department of Neurology
University of California
San Francisco, California

I. INTRODUCTION

A. Why the Ocular Motor Systems?

The ocular motor systems are ideal for studying the control of human movement. Eye movements are easy to measure, and the control of saccadic eye movements is simpler than the control of other neuromuscular systems. It is simpler because the load presented by the eyeball and extraocular tissues is small and constant. Horizontal eye movements offer a further simplification because they primarily involve only two muscles of each eye. By scrutinizing the trajectories of saccadic eye movements, we can infer the motoneuronal activity, deduce the central nervous system's control strategy, and observe changes in this control strategy caused by fatigue, alcohol, drugs, or pathology. These eye movement control principles should generalize to other neuromuscular systems.

There are two additional reasons for choosing the eye movement control systems as a model for neuromuscular control. First, we can present the development of a model by 11 authors over a span of more than 25 years (see Table 1). Second, an in-depth evaluation of this final model can be presented. The study of eye movement control models was chosen not because eye movements are thought to be so important, but rather because the physiological system is simple and typical and the models are well studied.[1]

B. Four Eye-Movement Systems

There are four types of eye movements: saccadic eye movements which are used for reading or scanning a scene, vestibulo-ocular movements which are used to maintain fixation during head movements, vergence eye movements which are used when looking between near and distant objects, and smooth pursuit eye movements which are employed when tracking moving objects, such as a high-flying bird.

These four types of eye movement are produced by four independent control systems. Their dynamic properties, such as latency, speed, and high-frequency cutoff values, are different. They are produced by different areas of the brain, and they are affected differently by fatigue, drugs, and disease.

The specific action of each system can be illustrated by considering a duck hunter sitting in a row boat on a lake. He scans the sky using saccadic eye movements. When he spots a duck he tracks it using smooth pursuit eye movements. When the duck comes closer to him, his eyes must move toward each other using vergence eye movements. While he is doing all of this, the boat is rocking which requires compensatory vestibulo-ocular eye movements. Thus all four control systems are continually used to move the eyes.

The model will work for all four types of eye movements, given the correct controller signals, but the saccadic system being the fastest presents the most stringent test of the model. Only controller signals for saccadic eye movements will be developed.

Saccade is a French word meaning fast jerk, as of a horse's reins. It was first applied to eye movements by Javal in 1879,[2] when he used the term to describe the rapid eye movements used during reading. The purpose of these saccadic eye movements is to place the high-resolution fovea, the central ½° of the retina, on the important features of the scene by using information from the periphery of the retina to direct the movement. However, we would not want our eyes to be continuously producing saccadic eye movements because we do not see well during saccades. For example, if you move your eyes between two points in the front of the room, you do not see the world rushing past, although the image on your retina is this moving scene. We have a process that suppresses our visual acuity during saccadic eye movements. This process, called saccadic suppression, is specific for saccadic size and direction.[3,4] Its effect can also be easily demonstrated by a simple experiment with a mirror. Look at the image of one of your eyes, then look at the image of the other eye. The rapid movement of the image during the saccade and the movements of the eyes were not seen because vision was partially suppressed during the saccade. Saccadic suppression is specific to the saccadic eye movement system.

II. THE MODELS

A. Descartes

An initial step in understanding this movement control system is the development of an appropriate descriptive model. One of the first eye movement models was developed by Descartes in 1630[5] to illustrate his discovery of the principle of reciprocal innervation. He thought that muscles behaved like balloons; when inflated they would be short and fat, when drained of fluid they would be long and skinny. The pipes in Figure 1 were used to pump fluid reciprocally in and out of the muscles.

B. Quantitative Eye Movement Models

1. Linear Second-Order System

The first control system model for the human saccadic eye movement system was proposed by Westheimer in 1954.[6] He recorded 20°-saccades and suggested that they looked like the step response of a linear second-order system. He suggested the following equation as his model

$$a\ddot{\theta} + b\dot{\theta} + c\theta = T(t)$$

where *a*, *b* and *c* are constants and θ, $\dot{\theta}$, and $\ddot{\theta}$ represent, respectively, the angular eye position, eye velocity, and eye acceleration. The force applied to the globe by the extraocular muscles is represented by $T(t)$, the tension in the muscle. This equation can be expressed as

$$\frac{\theta(s)}{T(s)} = \frac{\omega_n^2/K}{s^2 + 2\zeta\omega_n s + \omega_n^2}$$
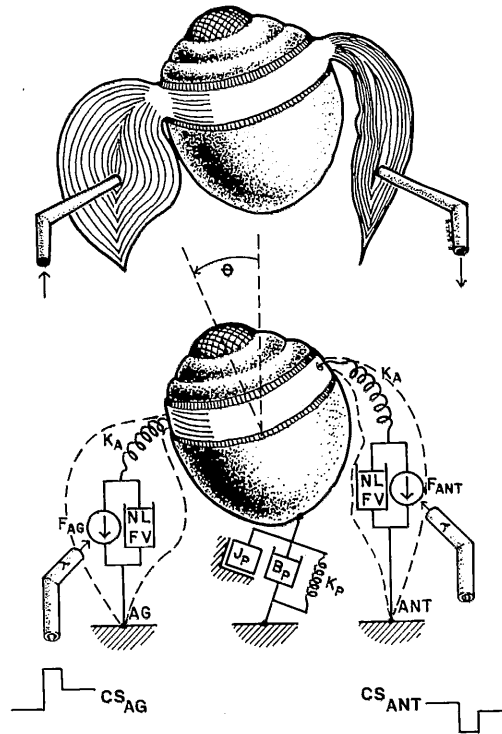
FIGURE 1. Two reciprocal innervation models for the human eye movement system. The top figure shows Descartes' basic concept of reciprocal action of muscles. Descartes thought that muscles were like balloons: when inflated they would be short and fat; when drained of fluid they would be long and skinny. The pipes were used to pump fluid reciprocally in and out of the muscles. Shortening of the agonist, together with lengthening of the antagonist, produces eye movements. The bottom figure shows the ideal mechanical elements used for modeling the plant. The globe and surrounding tissues were modeled by the inertia (J_p), a viscous element (B_p), and a passive elasticity. Each muscle was modeled by an active-state tension generator (F_{AG} and F_{ANT}), a nonlinear dashpot (NL-FV) representing the nonlinear force-velocity relationship, a series elasticity (K_A), and a parallel elasticity which was combined with the passive elasticity of the globe to form (K_p). The active-state tension generator converts motoneuronal firing into force through a first-order activation-deactivation process. The controller signals (CS_{AG} and CS_{ANT}) represent the aggregate activity of all of the motoneurons in the agonist and antagonist motoneural pools. (From Bahill, A. T., Hsu, F. K., and Stark, L., *Arch. Neurol. (Chicago)*, 35, 138, 1978. Copyright 1978, American Medical Association. With permission.)

Westheimer suggested that the values of zeta and omega were $\zeta = 0.7$ and $\omega_n = 120$.

The constant K would be the spring constant for a simple spring, mass dashpot system. Without loss of generality we can let $K = 1°/N$. The two major reservations that Westheimer had about his model were (1) that the real system was not linear because the peak velocity vs. magnitude plot was nonlinear (see Figure 2) and (2) that the force input was probably an exponential, not a step.
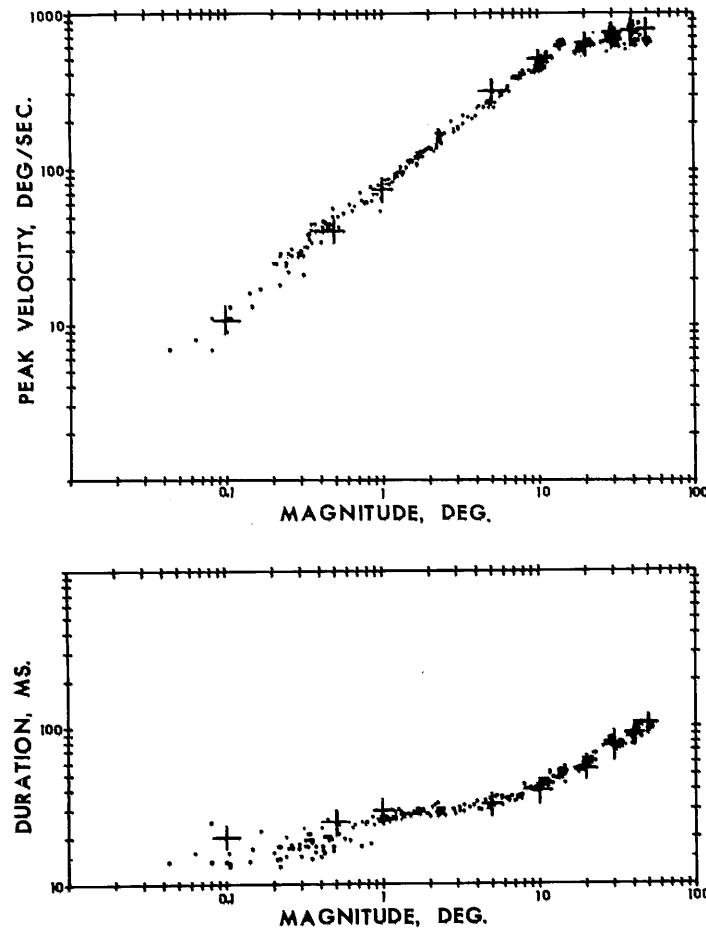
FIGURE 2.   Main sequence diagrams showing peak velocity (top) and duration (bottom) as functions of saccadic magnitude for normal human saccades (dots) and for the model (crosses). Human data were derived from eye position records with a 500-Hz bandwidth and eye velocity records with a 55-Hz bandwidth. (From Hsu, F. K., Bahill, A. T., and Stark, L., *Comput. Programs Biomed.*, 6, 108, 1976. With permission.)

After a model of a system has been developed, it is usually worthwhile to perform experiments on it. The model should be run in a variety of new modes. If any of these new situations yields interesting results, then similar experiments should be designed and performed on the physiological system. If the results of the model simulation and the physiological experiments are similar, then the validity of the model has been enhanced. As an example of this technique let us rederive and simulate Westheimer's model. The response of this linear second-order system to a step input is

$$\theta(t) = \Delta\theta \left[1 - \frac{e^{-\zeta\omega_n t}}{\sqrt{1 - \zeta^2}} \sin\left[\omega_n \sqrt{1 - \zeta^2}\, t + \phi \right] \right] \qquad (1)$$

where $\Delta \theta$ is the size of the saccadic step, and

$$\phi = Tan^{-1} \frac{\sqrt{1 - \zeta^2}}{\zeta}$$

What are the implications of this result? For the values that Westheimer used for his model, the time to peak becomes

$$T_p = \frac{\pi}{120 \sqrt{1 - (0.7)^2}} = 37 \text{ msec}$$

The time to peak is a reasonable definition for the duration of a saccade. It is independent of the size of the input step; this is not in concert with the experimental data. Figure 2 shows the duration as a function of magnitude for normal human saccadic eye movements. The duration increases with saccade size; therefore, the model fails to fit these data. The theoretical values of ζ and ω_n chosen by Westheimer yielded duration values that were only appropriate for a 10° saccade.

A comparison can also be made between the peak velocities of the model and the human data. To do this, we can twice differentiate Equation 1, set the result equal to zero, and solve for t. The time of maximum velocity becomes

$$T = \frac{n\pi + \phi}{\omega_n \sqrt{1 - \zeta^2}}$$

setting n = 0 and substituting into the velocity equation yields

$$\max \left[\frac{d\theta}{dt} \right] = \Delta \theta \frac{\omega_n}{\sqrt{1 - \zeta^2}} \sin\phi \ e^{-\phi/Tan\phi}$$

For $\zeta = 0.707$, $\phi = 45$ deg and $\dot{\theta}_{max} = 55 \Delta \theta$.

The second derivative test shows that this is indeed a maximum. This value of the peak velocity is directly proportional to the size of the input step. The human saccadic peak velocity data can be fit with a linear approximation only for saccades 15° and smaller. There is a soft saturation for larger magnitudes as shown in Figure 2. Therefore, the model does not match the physiological data. Westheimer noted this deficiency in his original model.

In summary, the step response of a linear second-order system has the same duration for all input magnitudes, and the peak velocity is directly proportional to the size of the input step. Because the human eye movement system has neither of these properties, we can conclude that this is a valid model for saccadic eye movements of only one size. In spite of its deficiencies, this model continued to be used (see, for example, Young and Stark)[7] until Robinson's model supplanted it in 1964.[8]

2. The Pulse-Step Input

Westheimer assumed that there was a step input to the extraocular muscles. In 1964, Robinson[8] performed an experiment to investigate this assumption. He applied a suction contact lens to the eye and then held the lens so that the eye could not move. He then measured the force required to hold this eye stationary while the other eye executed a saccade. Because the same innervation is sent to both eyes, he could infer the

AG

ANT
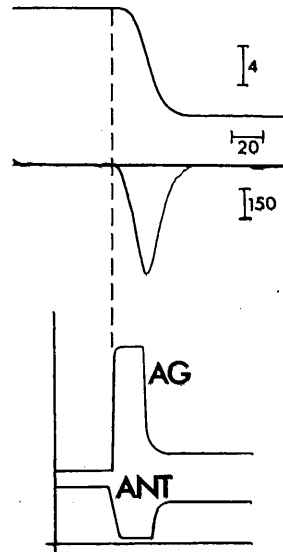
FIGURE 3. Eye position as a function of time (top) and eye velocity as a function of time (middle) for a typical saccade. Calibrations represent 4°, 20 msec, and 150°/sec. The pulse-step motoneuronal controller signals that are used to generate saccades represent the average motoneural activity of agonist (AG) and antagonist (ANT) as functions of time. The pulse is the high-frequency burst of neuronal firing that drives the eye rapidly between points. The step is the steady-state firing level that holds the eye in its new position. No time delay is shown between the start of the controller signal and the beginning of the saccade because this delay depends upon where the controller signal is measured.

muscle force responsible for the eye movement. This muscle force was a *pulse-step* similar to that shown for the agonist in Figure 3. At the motoneuronal level, the pulse corresponds to the high-frequency burst of motoneuronal firing that moves the eye rapidly from one position to the next, and the step corresponds to the steady state firing rate that holds the eye in its new position.

Robinson also increased the complexity of the model to that of a fourth-order system. His model then consisted of a pulse-step input signal and the following transfer function:

$$\frac{\theta_{eye}}{T} = \frac{0.667\,(0.02s + 1)}{(0.3s + 1)(0.06s + 1)(1.03 \times 10^{-5}s^2 + 0.004s + 1)}$$
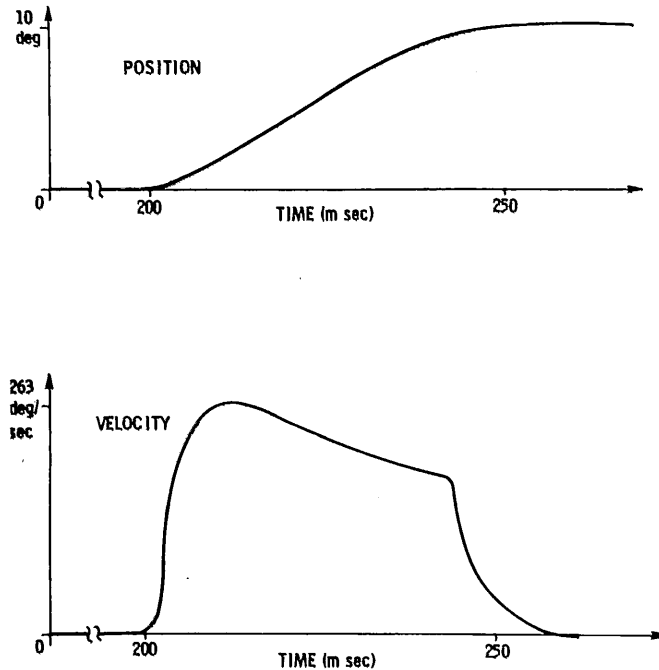
FIGURE 4.   Position and velocity curves from Robinson's model. The position curve is similar to human records, but the velocity profile has an abnormal knee near the end. (From Cook, G. and Stark, L., *Commun. Behav. Biol. Part A*, 1, 197, 1968. With permission.)

The numerical values were estimated from experimental data obtained from cats and were then adjusted by trial and error to match the human eye movement data.

This model could simulate saccades over a range of magnitudes between 5 and 40° by changing the size of the pulse and step. The input to this model was a force that was hypothetically proportional to the difference of the forces generated by the agonist and antagonist muscles. The position vs. time traces from Robinson's model matched his data fairly well. However, the velocity vs. time records had abrupt inflection points (see Figure 4) that did not occur in the physiological data.

3. The Homeomorphic Model

The reciprocal innervation model developed by Cook and Stark in 1968[9] and improved by Clark and Stark,[10] Bahill et al.,[11] and Hsu et al.[12] differed from Robinson's in two major ways. First, the duration of their pulse was not as long as the duration of the saccade. Second, they modeled the antagonist muscle as a separate independent entity, implementing Descartes' principle of reciprocal innervation. The big improvement in their model was its capability of producing realistic records of velocity as a function of time. The following development of the linear homeomorphic model is similar to Cook and Stark's, but it explicitly includes the effects of the length-tension diagram, and it incorporates the results of more recent physiological experiments on the muscle force-velocity relationship.

This marks the advent of the homeomorphic models where there is a one-for-one correspondence between the elements of the mode and elements, or effects, in the physiological system. So now, rather than discuss the evolution of whole models, let us investigate the development of individual elements of the model. The physiology

and experiments underlying the development of these elements are treated in greater detail by Bahill.[13]

a. The Passive Elasticity

Resting muscle is elastic. It can only be stretched by applying a force. The greater the force, the greater the extension (see curve labeled PM in Figure 5). Human physiological data are available for estimating this parameter for human eye movements.[14-16] Passive muscle is nonlinear, but for simplicity, the *passive elasticity* was modeled with an ideal linear spring. The coefficient K_{PE} was chosen so that the linear approximation yielded a reasonable fit to the data in the region of interest for the model.

b. Stimulus Response Relationship

A muscle produces a force when it is stimulated. A typical striated muscle responds to a single adequate stimulus with a twitch, a brief period of contraction followed by relaxation. The size and time course of the twitch depends upon the temperature, the particular type of muscle, and the strength of the stimulus. With very weak stimuli, nothing happens. When the stimuli exceeds threshold, a small response results. When the stimuli increases further, the response increases until it reaches a saturation limit. A reasonable explanation for this behavior is that the weak shock stimulates only a few muscle fibers close to the electrodes where the current density is highest, while the supramaximal shock stimulates all of them. [17]

If a second shock is given to the muscle before the response to the first has completely died away, summation occurs. If the stimuli are repeated regularly at a sufficiently high frequency, called tetanic stimulation, then a smooth tetanus results with tension maintained at a high level for as long as the stimulus train continues or until the onset of fatigue.[17]

An *ideal force generator* is used in the model to simulate this force-generating capability.

c. The Series Elasticity

The next element to be added to the model is the *series elasticity*. The effects of this element were demonstrated by the quick release experiments of Levin and Wyman in 1927:[18]

1.   A weight was hung from a muscle.
2.   The muscle was stimulated tetanically.
3.   The weight was quickly released.
4.   The muscle length and force were recorded as functions of time.

When the weight was released, the force abruptly decreased (because there was less of a load to support), and the muscle quickly shortened. There is an ideal mechanical element which will change its length instantaneously in response to an instantaneous change of force: a spring. For the model, this spring must be in series with the force generator; therefore, it is called the *series elasticity*. In the body, most of this elasticity is located in the tendon and in the actin and myosin cross bridges of the muscle.[19] The spring should be nonlinear,[20,21] but for small movements it can be approximated as a linear spring. Numerical data from human subjects show that K_{SE} is approximately 125 N/m (2.5 g tension per degree).[15]

It now becomes important to define precisely where the force is being measured. The force exerted by the tendon on the mass will be called the *muscle force* or *muscle*
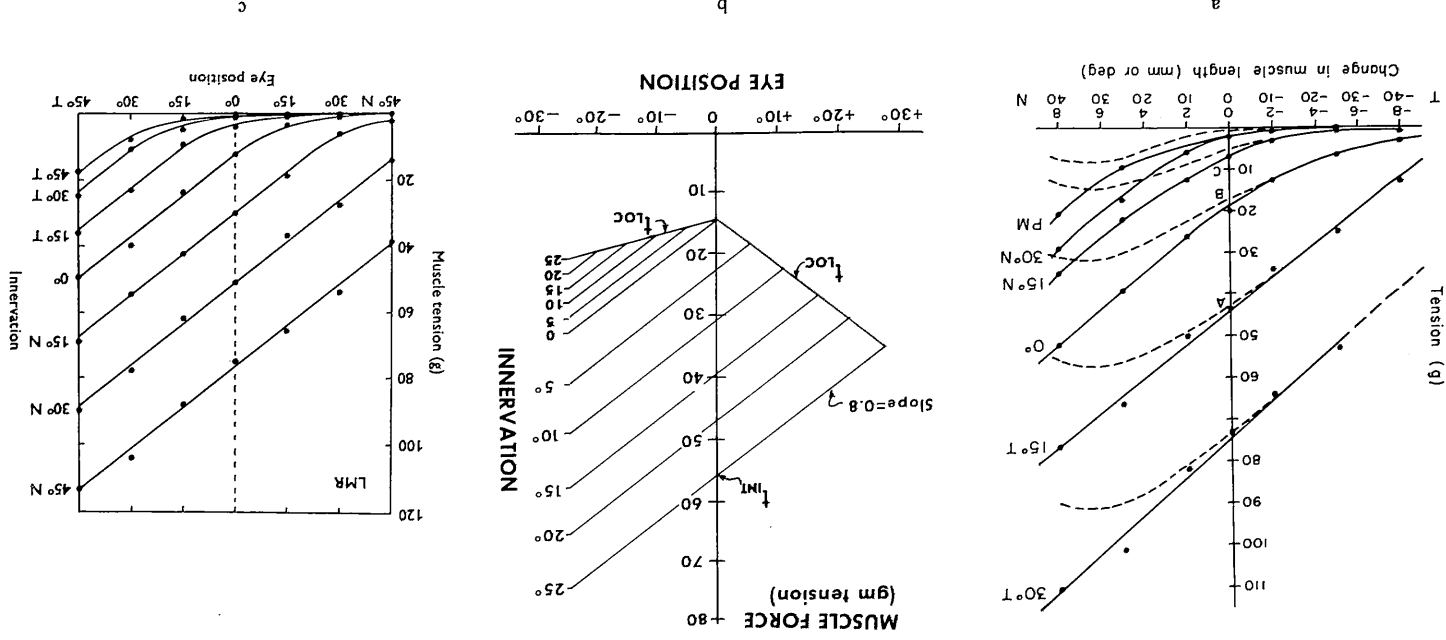
FIGURE 5. Length-tension curves for human extraocular muscle (a and c). The data were collected during strabismus surgery. The muscles were detached and then reattached to the eyeball in a different position. Before the muscles were reattached the patient was instructed to look at certain targets with his unoperated eye while the horizontal muscle of the operated eye was stretched to each of the indicated positions. The resulting force was then recorded. For example, in (a) when the operated eye was held in a position 10° nasal of primary position and the subject was asked to look at a target 15° temporal of primary position, a force of 50 g was developed by the lateral rectus muscle of the operated eye. The curve labeled PM is for passive muscle. When its effects are subtracted away, the forces of the active-state tension generator result (dashed lines). Part a from Robinson, D. A., O'Meara, D. M., Scott, A. B., and Collins, C. C., J. Appl. Physiol., 26, 548, 1969. With permission. (Part c from Collins, C. C., O'Meara, D., and Scott, A. B., J. Physiol., 245, 351, 1975. With permission.) (b) The linearized approximation which was used to derive the model parameters. The area below the curves is not entered by normal humans.[37]

a

Change in muscle length (mm or deg)

Tension (g)

PM   30°N   15°N   0°   15°T   30°T

b

EYE POSITION

INNERVATION

MUSCLE FORCE (gm tension)

slope=0.8   LOC   INT

c

Eye position

Innervation

Muscle tension (g)

LMR
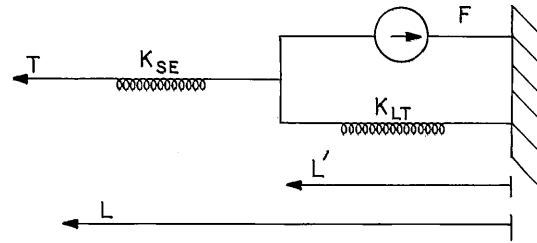
FIGURE 6. Muscle model with elements representing the effects of the length-tension diagram, K_{LT}, the series elasticity, K_{SE}, and the active state tension generator, F. The total force exerted by the muscle is T. The muscle length is L.[37]

tension and will be given the symbol T. The force from the ideal force generator will be called the *active state tension* and will be given the symbol F, as shown in Figure 6. The physiological literature is not so unambiguous.

d. The Antagonist Muscle

So far our discussions have been limited to muscles which shorten when stimulated. However, for every muscle that is shortened there is, roughly speaking, an *antagonist muscle* which is being lengthened. This antagonist muscle has a great effect on the dynamics of the resulting movement. In the model, the inhibition of the antagonist has just as great an effect on the velocity and duration of a saccade as the high-frequency burst of activity for the agonist. Scott[22] described human saccadic eye movements with almost normal velocities which resulted from the action of only the antagonist (the agonist was paralyzed and could contribute no force). From now on, effects of both an agonist and an antagonist muscle will be considered.

e. Length-Tension Diagram

The maximum contractile force a muscle can generate depends, in part, on its length. Muscle force generated by a contracted muscle is smaller than the maximum possible force. The *isometric* experiments performed to investigate this effect produce data of muscle force as a function of muscle length, as shown in Figure 5. The linearity, constant slope, and parallel lines of these length-tension diagrams can be explained by the sliding-filament model for muscle.[17,23]

The normal operating length of many muscles is near the region of maximum muscle force. The muscle length that produces maximum muscle force is called L_o. While walking, most of the locomotory muscles in the cat hind limb operate within $\pm 5\%$ of L_o.[24] For such muscles the length-tension diagram can be approximated with a straight line of zero slope. Previous versions of the reciprocal innervation model[9-12] assumed that extraocular muscles also operated near L_o. So these models produced the same muscle force for any length, which made it appear that the length tension diagram had been ignored.

Physiological data (Figure 5) have shown that human extraocular muscles operate well to the left of the point of maximum force, at lengths less than L_o. In their normal operating range, length-tension diagrams for these muscles can be modeled as straight lines of slope K'. A different line is used for each different value of innervation.

The length-tension diagram can be simulated with the model of Figure 6. The force generator, F, is called the active state tension generator. The distance L' is a hypothetical reference length and L is muscle length. T is the tension in the muscle which is also the force exerted on the eye by the muscle. The static equations for equilibrium are

$$T = F + K_{LT} L'$$ (2)

$$T = K_{SE} (L - L')$$ (3)

We can solve for L' in Equation 3, substitute this into Equation 2 and rearrange to get

$$T = \frac{K_{LT} K_{SE} L}{K_{LT} + K_{SE}} + \frac{K_{SE} F}{K_{LT} + K_{SE}}$$ (4)

The above equation for length-tension will produce the straight lines of Figure 5. The slope of these curves, K', is given in the length-tension Equation 4 as

$$K' = \frac{K_{LT} K_{SE}}{K_{LT} + K_{SE}}$$

Since K_{SE} is approximately 125 N/m (2.5 g tension per degree,[15] and K' can be estimated from the graph of Figures 5a and 5c as 40 N/m (0.8g tension per degree), K_{LT} can be calculated.

$$K_{LT} = \frac{K_{SE} K'}{K_{SE} - K'}$$

$$K_{LT} = 60 \text{ N/m} = 1.2 \text{ g tension per degree}$$ (5)

The straight lines labeled T_{Loc} in Figure 5b depict the fixation forces for the stationary eye. This is the tension, T, required to hold the eye at various angles of gaze. It is the total force of the agonist necessary to counterbalance the antagonist and orbital forces. The location of the agonist fixation forces are given by

$$T_{LOC} = 14 + 0.8 \, \Delta \theta$$

The muscle tension axis intercept ($\theta = 0$), T_{INT}, is found by

$$T_{INT} = T_{LOC} + K' \Delta \theta = T_{LOC} + 0.8 \, \Delta \theta = 14 + 1.6 \, \Delta \theta$$ (6)

Another equation for T_{INT} can be obtained by setting $L = 0$ in Equation 4 to yield

$$T_{INT} = \frac{K_{SE} F}{K_{LT} + K_{SE}}$$ (7)

The force F is that produced by the active-state tension generator. For the steady-state behavior of the agonist muscle, this force is the same as the neural activity, $N_{AG-step}$. (The definition of $N_{AG-step}$ is illustrated in Figure 12.) Now Equations 6 and 7 can be combined to yield

$$14 + 1.6 \, \Delta \theta = \frac{K_{SE}}{K_{LT} + K_{SE}} \, N_{AG-STEP}$$

$$N_{AG-STEP} = \frac{(14 + 1.6 \, \Delta \theta) \, (K_{LT} + K_{SE})}{K_{SE}}$$

$$N_{AG-STEP} = (20.6 + 2.35 \, \Delta \theta) \, \text{g tension} \qquad (8)$$

The same steps can be performed for the antagonist.

$$T_{LOC} = 14 + 0.3 \, \Delta \theta$$

$$T_{INT} = T_{LOC} - 0.8 \, \Delta \theta = 14 - 0.5 \, \Delta \theta$$

$$14 - 0.5 \, \Delta \theta = \frac{K_{SE}}{K_{LT} + K_{SE}} \, N_{ANT-STEP}$$

$$N_{ANT-STEP} = (20.6 - 0.74 \, \Delta \theta) \, \text{g tension} \qquad (9)$$

f. The Force Velocity Relationship

The nonlinear force-velocity relationship is revealed by *isotonic* experiments. In these experiments, performed by Fenn and Marsh[25] in 1935, the muscle length is adjusted to be near rest length, then it is stimulated (usually to 100% activation). The load is then applied and the muscle is allowed to shorten. In this way, records similar to Figure 7c are obtained. It can be seen that the greater the load, the smaller the total shortening. In fact, force and final length follow the left-hand part of the length-tension curve for active muscle which was shown in Figure 5. Because the experiments are done isotonically, the length of the series elasticity will remain constant and the changes in the force will be due to modifications of the active-state tension. The numerical values for the force-velocity elements in the model match human data[15] but they were not derived directly from human experiments. If they were, then either these experiments would have had to be done with small changes in length or else the length-tension effects would have had to be calculated and subtracted off, in order to compensate for the effects of the length-tension elasticity. For this discussion, the most important effect of the force-velocity relationship is that as the load gets larger, the maximum speed of shortening gets smaller; that is, the maximum slope of the curve gets smaller. If force or load is plotted against slope, then a graph similar to the 100% activation curve of Figure 7a is obtained. Each curve in Figure 7c yields one data point for the 100% activation curve in Figure 7a.

Many different equations can be fit to the force-velocity data. The most interesting one is Hills equation[26] which fits part of a hyperbola to the curve.

$$V = \frac{(F_o - T)b}{(T + a)}$$

where V is the velocity, T is the muscle force, F_o is the isometric force, and a and b are constants for any given percentage of activation. Hill's experimental data suggested values of $a = \frac{1}{4} \, F_o$ and $b = \frac{1}{4} \, V_{max}$. The term V_{max} is a measurable parameter, the maximum muscle velocity for any particular percentage of activation. The symbol F_o is used to represent the muscle force measured at zero velocity. For these isotonic

MUSCLE FORCE

100% activation

50%

5%

0 Vmax1   Vmax2   Vmax3   **Shortening
Velocity**

(a)
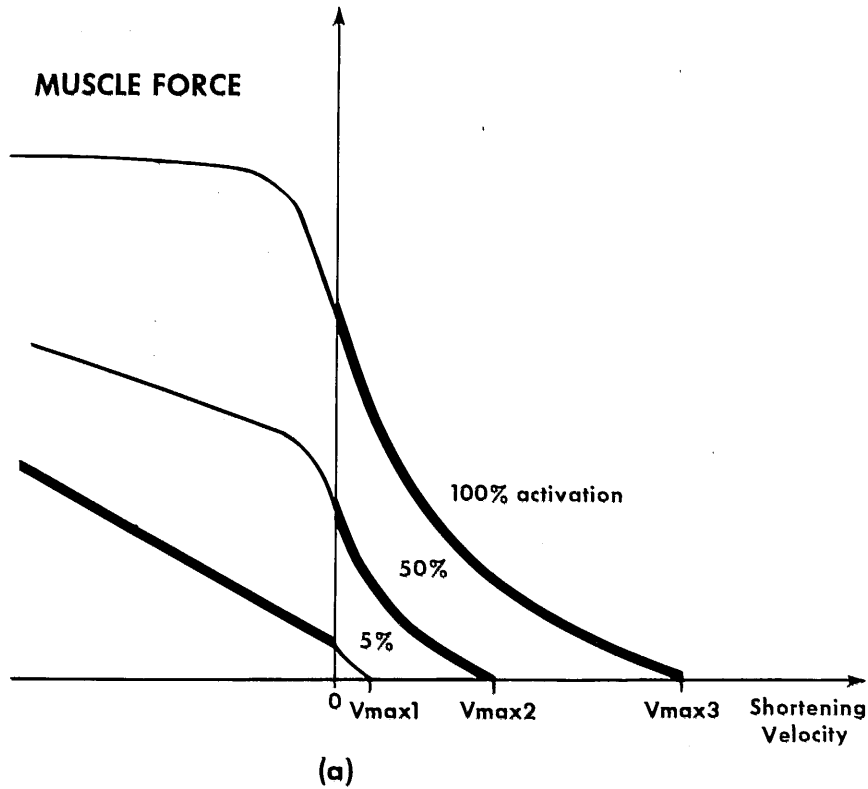
FIGURE 7.   Records of shortening as a function of time from a muscle lifting various loads (c). Tetanic stimulation started at time zero. These three experiments would provide three points for the 100% activation curve for the force-velocity relationship (a).[17,20] There is a family of curves for different activation states. The force-velocity relationship for muscles is hyperbolic, but the curves can be approximated with straight lines (b). The curves in the first quadrant are for the agonist muscle, and the curves in the second quadrant are for the antagonist muscle. Agonist activation is typically between 50 and 100% activation. Antagonist activity is typically less than 5% activation. The antagonist curve for 5% activation is best fit with only one straight line. The thick lines indicate the normal operating regions during saccades.[41]

experiments, F_o is the active-state tension. This parameter depends upon the degree of activation of the muscle; that is, F_o for 100% activation is larger than F_o for 50% activation. Although in the experiments described, muscle force (or load) is the independent variable, the curves are usually plotted with muscle force on the ordinate. Hills equation can be rearranged as

$$T = F_o - \left[\frac{F_o + a}{b + V}\right] V$$

and therefore

$$T = F_o - BV$$

Where
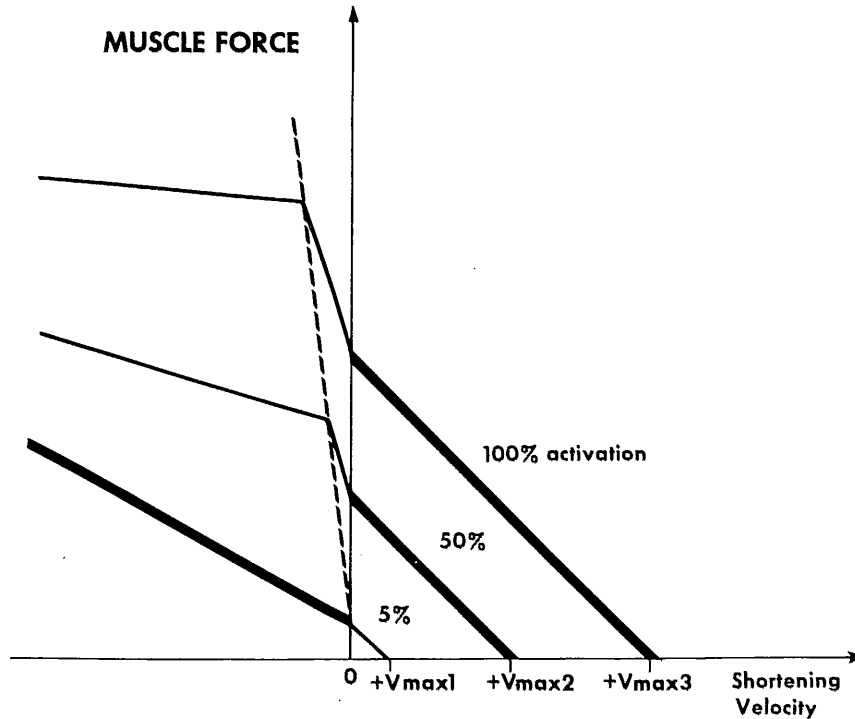
MUSCLE FORCE
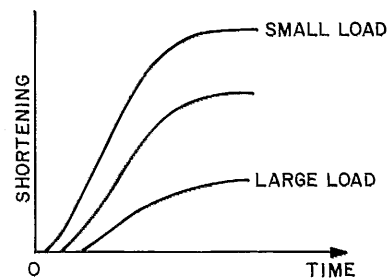
Figure 7b

Figure 7c

$$B = \frac{F_o + a}{b + V}$$

The force-velocity relationship shows that muscles produce larger forces at lower velocities. It is as if there were an internal dashpot absorbing some of the force available from the active state tension generator. This is just how this relationship is modeled in Figure 8. The muscle force available at the tendon is decreased by a velocity-dependent term, an apparent viscosity.

The force-velocity relationship of a muscle which is being lengthened is quite different from that of a muscle which is allowed to shorten.[27-33] The antagonist muscle is usually activated only slightly, yet it offers a large resistance to being stretched. It is possible to use the same function, a hyperbola, to model the antagonist force-velocity relationship as shown in Figure 9. Hsu et al.[12] used these curves; replaced F_o with the
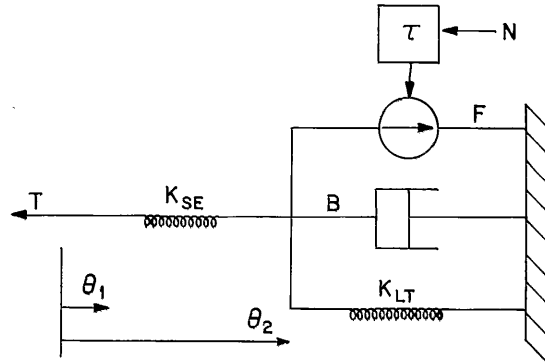
FIGURE 8. Muscle model with addition of nonlinear force-velocity relationship, B. The neuronal controller signal is represented by N. This signal is transformed into active state tension, F, by an activation or deactivation time constant, τ.[37]
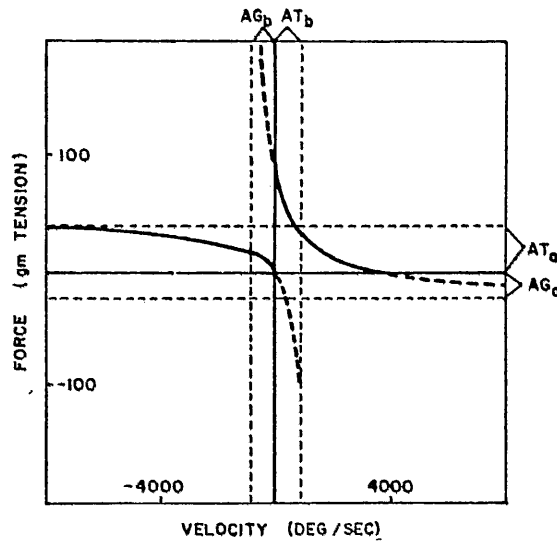
FIGURE 9. Force-velocity relationships for both the agonist and the antagonist muscles can be represented by hyperbolas of similar form. These curves are appropriate for a 10° saccade. (From Hsu, K. H., Bahill, A. T., and Stark, L., *Comput. Programs Biomed.*, 6, 108, 1976. With permission.)

active state tensions, F_{AG} and F_{ANT}; replaced a with AG_a and ANT_a, respectively, for the agonist and antagonist muscles; replaced b with AG_b and ANT_b, respectively, for the agonist and antagonist muscles; replaced the linear velocity, V, with angular velocity $\dot{\theta}$; and derived the following functions for the agonist and antagonist dashpots

$$B_{AG} = \frac{F_{AG} + AG_a}{\dot{\theta}_2 + AG_b}$$

and

$$B_{ANT} = \frac{F_{ANT} - ANT_a}{\dot{\theta}_3 - ANT_b}$$

Numerical values for the force and velocity axes intercepts are unique for each muscle. The velocity axis intercept, $v_{max} = 4b$, is the maximum isotonic contraction velocity for the muscle under study. The previous models[9-12] derived this constant from cat experiments. They used 3600°/sec for the velocity axis intercept, v_{max}. This value is four times larger than the maximum recorded human extraocular eye muscle velocity and is more than twice as large as the maximum velocity of θ_2 in the model. The sensitivity analysis[12] showed that this parameter was the third most important parameter in the model. Accordingly, this parameter was reformulated in subsequent models.

Nonlinearities of the models were due to this nonlinear force-velocity relationship which was modeled as a nonlinear dashpot. Clark and Kamat (in Reference 34) tried to linearize the model by using a Taylor series expansion on the model (excluding second and higher order terms). The linear pertubation equations were not trivial to solve, and the implementation of a known nominal solution was cumbersome. The oversimplification of neglecting the activation and deactivation time constants was the most likely reason that their linear model did not match physiological data. In another effort to linearize the model, Latimer et al.[35] plotted numerical values for the dashpots representing the apparent viscosities of the muscles. Straight-line approximations of these time functions closely fit the actual values of the dashpots for a 10° saccade. The nonlinear problem was thereby transformed into a time variant problem, which was still cumbersome.

The most obvious method of linearizing is to approximate the force-velocity curves with straight lines. Stark,[36] in formulating the BIOSIM simulation language, approximated these curves with straight lines through a single point labeled V_{max3} in Figure 7b. This linearized the force-velocity relationship but did not linearize the model because the dashpot parameters became functions of the model states.[35] Additional physiological data[29-33] have shown that V_{max} is not constant, but depends upon the percentage of activation, as shown in Figure 7. By incorporating this additional data, Latimer et al.[35] were able to linearize both the force-velocity relationship and the homeomorphic sixth-order model. This linearization scheme was subsequently used in later models.[37,38]

g. Parameter Estimation

In developing a model of a system, the parameters of the mode must be assigned numerical values. Sometimes this assignment can be made based upon knowledge of the physical system. For example, the mass of an object being controlled is often known. However, some physical parameters, such as the viscosities in the reciprocal innervation model, can only be estimated. Choosing parameter values can be done manually or under computer control.

So far in this paper all parameter fitting has been done by eye. For example, the experimental passive length-tension diagram of Figure 5 was approximated with a hand-drawn straight line. This approximation was then used in the construction of the model. Other parameters, such as the agonist activation time constant, were adjusted after the model was constructed. The model was run and the output was visually compared to human eye movements. Then the time constant was changed and the model was run again. After many iterations, a satisfactory value of the parameter was obtained.
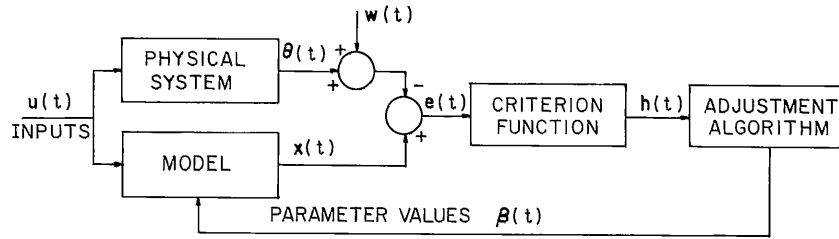
FIGURE 10. To find the optimal model parameters both the model and the physical system are excited with the same input, u (t). The two outputs, θ (t) and x (t), are compared and the difference between the two, the error e (t), is used to form the criterion function, h(t). The adjustment algorithm iteratively changes the parameter values, β (t), until the criterion function is minimized. Appropriate steps may be taken to account for measurement noise, w(t).[41]

A digital computer can perform this parameter estimation more efficiently. Figure 10 shows the estimation scheme. The criterion function is the mean squared error between the model and plant outputs. It is a function of the parameter values, β.

$$h(\beta) = \frac{1}{T} \int_0^T (x - \theta)^T G (x - \theta) \, dt$$

The superscript T represents the matrix transpose operation and G is a weighting matrix. For the simple example presented in the next section G $= 1$, and only one variable, the model output, is studied. The criterion function becomes

$$h(\beta) = \frac{1}{T} \int_0^T (x_1 - \theta_1)^2 \, dt$$

The purpose of the algorithm is to adjust the parameters so as to minimize this function. Many function minimization programs can be used for this purpose.[39,40] The Davidson-Fletcher-Powell method is perhaps the most powerful, but it is also difficult to use. Latimer and Bahill[41] discussed several classical techniques and developed a modified steepest descent technique for function minimization. This technique allowed several parameters to be varied simultaneously and also allowed several outputs to be compared.

This technique was used to determine the values of the agonist and antagonist dashpots and of the time constants that would yield the least mean squared error between the model output and eye position during a human saccade. The method was very powerful. Almost all changes in the saccadic trajectories that were not produced by input signal variations could be matched by small parameter changes. The parameter estimation routine was used to find optimal values for agonist and antagonist dashpots in the model.

h. Derivation of Numerical Values for the Force-Velocity Relationship

Previous models have been nonlinear because the force-velocity data were fit with a family of hyperbolas through a fixed point on the velocity axis (v_{max}). However, physiological data have shown that V_{max} varies with the percentage of activation.[29-33] Thus, a better linearization would be a family of piecewise linear curves with equal constant slopes, as shown in Figure 7b.

When a muscle is stimulated and quickly stretched, it offers a high resistance to the external force. This antagonist force-velocity relationship can be modeled by a two-piece linear approximation as shown in the left side of Figure 7b. The intersection of these two lines is a linear force-dependent function. During normal saccadic move-ments the antagonist muscle force is reduced, corresponding to less than 2% of maximum innervation. The parameter estimation algorithm[41] was used in an attempt to find the intersection and slopes of the piece wise linear approximations of the force-velocity curves using a 10° saccade. The results showed that the best fit to the data was obtained by using only one line for the force-velocity approximation of the 2% innervation curve for the antagonist muscle.[41] This unexpected result greatly simplified the linearization of the force-velocity relationship.

The parameter estimation routine produced the following constant slopes for the force-velocity relationship

$$B_{AG} = 2.36 \text{ N–s/m} = 0.046 \text{ g tension–sec/}°$$

$$B_{ANT} = 1.12 \text{ N–s/m} = 0.022 \text{ g tension–sec/}° \tag{10}$$

In a previous section, Equation 4 was derived. It represented the force available at the tendon after the active-state tension was modified by the effects of the length-tension diagram. To make this equation appropriate for rotations, a new variable θ_1 is defined in Figure 8. Its value will be zero when the eye is in primary position (looking straight ahead). For variations about this operating point $\theta_1 = -L$. Thus Equation 4 becomes

$$T = \frac{K_{SE}F}{K_{LT} + K_{SE}} - \frac{K_{LT}K_{SE}\theta_1}{K_{LT} + K_{SE}}$$

We must now decrement this available force to account for the effects of the force-velocity relationship. The muscle force available at the tendon becomes

$$T = \frac{K_{SE}F}{K_{LT} + K_{SE}} - \frac{K_{LT}K_{SE}\theta_1}{K_{LT} + K_{SE}} - B_{AG}\dot{\theta}_2 \tag{11}$$

i. The Passive Tissues and the Eyeball

The rotational inertia of the eyeball is represented by J in Figure 11. The eyeball has been modeled as a solid sphere of ice with a radius of 11 mm. A much more complicated model using several concentric spheres connected by visco-elastic elements could have been used, but sensitivity analyses of the models showed that this was unnecessary.[12,42]

The optic nerve, the other extraocular muscles, orbital fat, check and suspensory ligaments, and other tissues contribute to the visco-elasticity which limits the movement of the eyeball. Human physiological data are available for evaluating these parameters.[14-16] They are modeled by a spring and a dashpot, K'_P and B_P. Although some modelers have used two groups of springs and dashpots in series for such elements, the sensitivity analyses [12,42] proved this added complication unnecessary.

The new model is shown in Figure 11. The spring K_P represents the total passive elasticity of the orbit and surrounding tissues and of the agonist and antagonist muscles. This model is said to be a homeomorphic model because there is a one-to-one relationship between the elements of the model and the elements of the physiological system. Such a similarity of form makes evaluation of a model easier.
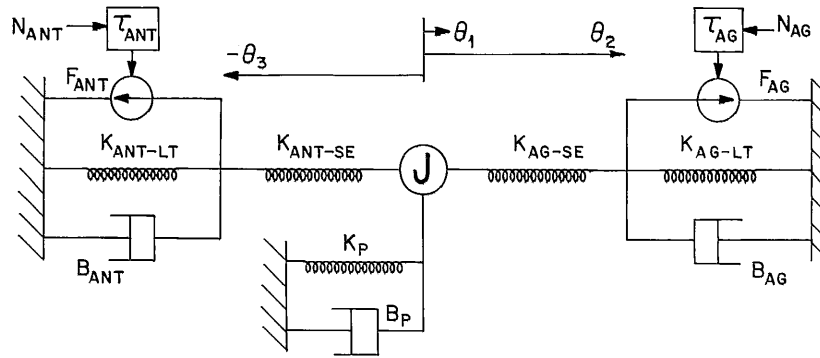
FIGURE 11.   Linear homeomorphic model of the extraocular plant. θ_1 is the distance of the eye from primary position (0°). θ_2 is the distance of the agonist node from primary position. It is separated from θ_1 by the agonit series elasticity. θ_3 is the distance of the antagonist node from primary position. This model differs from that shown in Figure 1 in that the model is linear, and it includes the effects of the muscle length tension diagram. (From Bahill, A. T., Latimer, J. R., and Troost, B. T., *IEEE Trans. Biomed. Eng.*, BME-27, November 1980. With permission.)

j. Activation and Deactivation Time Constants

As shown in Figure 12, muscle force does not rise to its maximum value instantaneously: even the active state tension does not rise to its maximum value instantaneously. However, the ideal pulse-step controller signal used to produce saccadic eye movements does rise instaneously. In the reciprocal innervation model, the idealized pulse-steps were modified by first-order lag circuits (low-pass filtering) in order to produce the active state tensions of the muscles.

$$F_{AG} = N_{AG}(1-e^{-t/\tau})$$

$$F_{ANT} = N_{ANT}(1-e^{-t/\tau})$$

These tensions were then modified by the nonlinear force-velocity relationships, by the effects of the length-tension diagrams, and by the series elasticities to produce muscle forces (see Figure 12).

In the physiological system, there is both a delay and a low-pass filtering in the transition between the pulse-step and the active-state tensions. The model does not include the delay between the onset of the pulse and the start of the saccade, because this delay is not fixed: it depends upon where the pulse-step is measured. The model does include the filtering. Physiologically, this filtering is due to both spreading in time and rate-limiting factors. The spreading is due to variations between cells in synchronization, synaptic transmission delays, motoneuronal firing frequency acceleration, neuronal conduction velocity, depolarization, spread of activity in the sarcoplasmic reticular formation, and acceleration of the moysin cross bridges. The rate-limiting processes include the synaptic transmissions, the release and reuptake of the Ca^{++}, and its modification of the actin-myosin fibers. For simplicity, we have accounted for all of these with simple first-order time constants defined in Figure 12.

Most of this low-pass filtering is probably due to the Ca^{++} activation process. A clue for a physiological value of this time constant can be taken from studies[43] of the frog with a Ca^{++}-sensitive bioluminescent protein which emitted light in the presence of calcium ions. The muscle was electrically stimulated, and the light flux vs. time was plotted. From these data, a 10% to 90% rise time of 7 to 20 msec was calculated (for
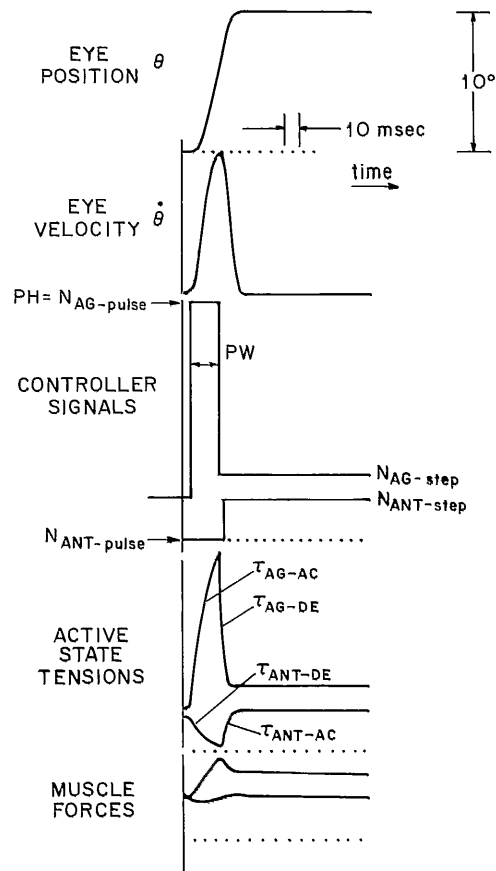
FIGURE 12. Signals involved in the transformation of input commands into eye movements. The pulse-step controller signals have abrupt transitions which are filtered out by the activation and deactivation time constants to produce the active state tensions. These are in turn filtered by the series elasticity, the length-tension elasticity, and the force-velocity relationship to produce the forces that are applied to the globe. These forces produce the eye movements.[13]

frog muscle at 15°C). Adjusting this value for 25°C (division by 2.2) yields 3 to 9 msec. Changing this into time constants (division by 2.2) yields 2 to 4 msec. These values were fine tuned by using them in the model and by comparing model data to human physiological data. The time constants that were finally used ranged between 0.2 and 12 msec.

At least one of these time constants, τ_{AG-AC}, is a function of motoneuronal firing frequency. This hypothesis is supported by two separate arguments. The first is that the rate of muscular tension development increases with higher motoneuronal firing frequencies. This has been offered as an explanation for oculomotoneurons firing at frequencies that were higher than the muscle tentanus frequency. Although maximum tension will not continue to rise with increasing frequency, the rate of tension rise will increase. This proportionality between rate of tension development and motoneuronal firing frequency has been demonstrated for lateral rectus muscles,[44] for fast units of

the inferior oblique muscles,[45] and for slow units of the soleus muscle.[46] Larger movements are produced by, among other things, higher motoneuronal firing frequencies. Therefore, larger movements should have a faster rate of tension rise. This phenomenon is probably related to the facilitation of the second of a pair of closely spaced neuronal spikes and is similar to the catch property of certain invertebrate muscles.[47] The way this relates to the time constant is that in large saccades the motoneurons fire at higher frequencies and yield faster rates of tension rise. This is modeled with a smaller time constant.

The second reason for time constant variability is that muscle fibers have different properties. Some are fast and some are slow. The slow fibers contract slowly, but resist fatigue. They are the tonic fibers. Each fiber is small and contributes a small amount to the total muscle force. The fast fibers contract rapidly and fatigue quickly. They are the phasic fibers. Each fast fiber is larger and contributes much more force than a slow fiber. Some muscles are composed predominately of fast fibers, some predominately of slow fibers, and some of an intermediate mixture.

Large saccadic eye movements will recruit the large, fast, fast-fatiguing, global fibers (those nearest the globe), whereas small saccades will only recruit the smaller and slower orbital fibers (those nearest the orbit).[15] Therefore, because the larger saccades recruit the faster motoneurons, the rate of rise of muscle force should be greater for larger saccades.

Lacking physiological evidence to the contrary, the agonist deactivation time constant and both of the antagonist time constants were fixed for all size saccades. Only the agonist activation time constant was made a function of saccadic size.

Initial starting values for these parameters were chosen from the reciprocal innervation model of Hsu et al.[12] Then the parameter estimation program was run with the four time constants free to vary. The values that gave the least mean squared error between the model and human outputs were used for the final model.

k. Antagonist Circumscription

The antagonist activity circumscribes the agonist activity (see Figures 3 and 12). Electromygraphic (EMG) studies have shown that the antagonist resumes its activity after the agonist ceases its burst of activity.[15] It has been reported that the pause of the antagonist motoneuronal pool starts before the agonist motonuronal pool begins its high-frequency burst of firing in the lateral and medial rectus muscles of humans,[48] the abducens motoneurons,[49,50] the trochlear motoneurons,[51] the pausing and bursting units within the reticular formation that are associated with saccades,[52] and in arm muscles.[53] In the model the antagonist activity ceases 3 msec before and resumes 3 msec after the agonist activity.

l. The Plant and System Equations

The linear homeomorphic model can now be derived with reference to Figure 11. Two muscles are pulling in opposite directions on the globe, J. Their forces are

$$T_{AG} = K_{SE}(\theta_2 - \theta_1) \tag{12}$$

$$T_{ANT} = K_{SE}(\theta_1 - \theta_3) \tag{13}$$

From Equation 11,

$$T_{AG} = \frac{K_{SE} F_{AG}}{K_{LT} + K_{SE}} - \frac{K_{LT} K_{SE} \theta_1}{K_{LT} + K_{SE}} - B_{AG} \dot{\theta}_2 \tag{14}$$

and

$$T_{ANT} = \frac{K_{SE} \, F_{ANT}}{K_{LT} + K_{SE}} + \frac{K_{LT} K_{SE} \theta_1}{K_{LT} + K_{SE}} + B_{ANT} \dot{\theta}_3 \qquad (15)$$

Corresponding minus signs of Equation 14 are plus signs in Equation 15 because the antagonist dashpot adds to the resistive force of the antagonist active-state tension and also, as the muscle gets longer, the length-tension diagram perscribes more muscle force which increases the resistive force.

Now Equations 12 and 14 can be combined to yield

$$\frac{K_{SE} \, F_{AG}}{K_{LT} + K_{SE}} - \frac{K_{LT} K_{SE} \theta_1}{K_{LT} + K_{SE}} - B_{AG} \dot{\theta}_2 = K_{SE}(\theta_2 - \theta_1) \qquad (16)$$

and Equations 13 and 15 can be combined to yield

$$\frac{K_{SE} \, F_{ANT}}{K_{LT} + K_{SE}} + \frac{K_{LT} K_{SE} \theta_1}{K_{LT} + K_{SE}} + B_{ANT} \dot{\theta}_3 = K_{SE}(\theta_1 - \theta_3) \qquad (17)$$

The two muscle forces acting on the globe (Equations 12 and 13) can be combined with the other forces acting on the globe to yield

$$K_{SE}(\theta_2 - \theta_1) - K_{SE}(\theta_1 - \theta_3) = K_p \theta_1 + B_p \dot{\theta}_1 + J \ddot{\theta}_1 \qquad (18)$$

Equations 16, 17, and 18 describe the movements of the model. However, the model is a sixth-order system, so it takes six differential equations to completely describe the system. For these state equations we will use the three positions, θ_1, θ_2, and θ_3, the eye velocity $\dot{\theta}_1$, and the two active-state tensions, F_{AG} and F_{ANT}. We identify these state variables with the symbols x_1 to x_6.

$x_1 = \theta_1$	= position of eye
$x_2 = \theta_2$	= position of agonist node, shown in Figure 11
$x_3 = \theta_3$	= position of antagonist node, shown in Figure 11
$x_4 = \dot{\theta}_1$	= eye velocity
$x_5 = F_{AG}$	= agonist active-state tension
$x_6 = F_{ANT}$	= antagonist active-state tension

The inputs to the model are the neural control signals N_{AG} and N_{ANT}. These signals are transformed into the active-state tensions by first-order activation and deactivation processes as shown in Figure 12.

The three simultaneous equations (Equations 16, 17, and 18) can be solved for each of the variables and three auxillary equations can be formed to yield the following six state equations:

$$\dot{x}_1 = x_4$$

$$\dot{x}_2 = \frac{K_{SE}^2}{(K_{LT} + K_{SE}) B_{AG}} x_1 - \frac{K_{SE}}{B_{AG}} x_2 + \frac{K_{SE}}{(K_{LT} + K_{SE}) B_{AG}} x_5$$

$$\dot{x}_3 = \frac{K_{SE}^2}{(K_{LT} + K_{SE})B_{ANT}} x_1 - \frac{K_{SE}}{B_{ANT}} x_3 - \frac{K_{SE}}{(K_{LT} + K_{SE})B_{ANT}} x_6$$

$$\dot{x}_4 = \frac{-2K_{SE}-K_p}{J} x_1 + \frac{K_{SE}}{J} x_2 + \frac{K_{SE}}{J} x_3 - \frac{B_p}{J} x_4$$

$$\dot{x}_5 = \frac{cN_{AG}-x_5}{\tau_{AG}}$$

$$\dot{x}_6 = \frac{cN_{ANT}-x_6}{\tau_{ANT}}$$

where c is a conversion factor with a value of 0.004 N-s per spike.
The initial conditions are

$$x_1(0) = x_4(0) = 0$$

$$x_2(0) = -x_3(0) = 1.1 \text{ mm} = 5.6°$$

$$x_5(0) = x_6(0) = 0.2 \text{ N} = 20.6 \text{ g tension}$$

These state equations completely describe the behavior of the model. It is sometimes more convenient to write these equations using matrix notation.

$$\dot{x} = Ax + Bu$$

In this equation $\dot{x}$, x, and u are vectors, B may be a vector or a matrix, and A is a square matrix. Using this notation our six state equations become

$$
\begin{bmatrix} \dot{x}_1 \\ \dot{x}_2 \\ \dot{x}_3 \\ \dot{x}_4 \\ \dot{x}_5 \\ \dot{x}_6 \end{bmatrix}
=
\begin{bmatrix}
0 & 0 & 0 & 1 & 0 & 0 \\
\dfrac{K_{SE}^2}{(K_{LT}+K_{SE})B_{AG}} & \dfrac{-K_{SE}}{B_{AG}} & 0 & 0 & \dfrac{K_{SE}}{(K_{LT}+K_{SE})B_{AG}} & 0 \\
\dfrac{K_{SE}^2}{(K_{LT}+K_{SE})B_{ANT}} & 0 & \dfrac{-K_{SE}}{B_{ANT}} & 0 & 0 & \dfrac{-K_{SE}}{(K_{LT}+K_{SE})B_{ANT}} \\
\dfrac{-2K_{SE}-K_p}{J} & \dfrac{K_{SE}}{J} & \dfrac{K_{SE}}{J} & \dfrac{-B_p}{J} & 0 & 0 \\
0 & 0 & 0 & 0 & \dfrac{-1}{\tau_{AG}} & 0 \\
0 & 0 & 0 & 0 & 0 & \dfrac{-1}{\tau_{ANT}}
\end{bmatrix}
\begin{bmatrix} x_1 \\ x_2 \\ x_3 \\ x_4 \\ x_5 \\ x_6 \end{bmatrix}
+
\begin{bmatrix} 0 \\ 0 \\ 0 \\ 0 \\ \dfrac{cN_{AG}}{\tau_{AG}} \\ \dfrac{cN_{ANT}}{\tau_{ANT}} \end{bmatrix}
$$

m. Parameter Values

The following parameter values are given to complete the description of this model. Equations 5, 8, 9, and 10 appear directly. The neural signals, N_{AG} and N_{ANT}, are given units of motoneuronal spikes per second for a typical motoneuron.

Initial values for pulse width, pulse height, and the four time constants were based upon the values used for 10° saccades in the old model. The parameter estimation

program was then run and these six parameters were adjusted to yield the least mean squared error between the model and human responses. These values were then fixed for 10° saccades. The parameter estimation routine was run again on a different size saccade adjusting pulse width, pulse height, and $\tau_{AG\text{-}AC}$ to minimize the error between model and human saccades. This procedure was repeated for saccades between 1 and 40°. Straight line approximations were then fit to these data points to yield the following equations:

$$K_{SE} \quad = 125 \text{ N/meter} = 2.5 \text{ g tension/}°$$

$$K_{LT} \quad = 60 \text{ N/m} = 1.2 \text{ g/}°$$

$$K_p \quad = 25 \text{ N/m} = 0.5 \text{ g/}°$$

$$B_P \quad = 3.1 \text{ N-s/m} = 0.06 \text{ g-sec/}°$$

$$B_{AG} \quad = 2.36 \text{ N-s/m} = 0.046 \text{ g-sec/}°$$

$$B_{ANT} \quad = 1.12 \text{ N-s/m} = 0.022 \text{ g-sec/}°$$

$$J \quad = 2.2(10^{-3}) \text{ N-s/m} = 4.3(10^{-5}) \text{ g-sec}^2/°$$

$$N_{AG\text{-}PULSE} \quad = PH = (135 + 27 \Delta\theta) \text{ spikes/sec for } \Delta\theta \leq 11°$$

$$= (392 + 5 \Delta\theta) \text{ spikes/sec for } \Delta\theta > 11°$$

$$N_{ANT\text{-}PULSE} \quad = 1.2 \text{ spikes/sec}$$

$$PW_{AG} \quad = (10 + \Delta\theta) \text{ msec}$$

$$PW_{ANT} \quad = PW_{AG} + 6 \text{ msec}$$

(Antagonist pulse starts 3 msec before and ends 3 msec after agonist pulse)

$$N_{AG\text{-}STEP} \quad = (50.1 + 5.5 \Delta\theta) \text{ spikes/sec}$$

$$N_{ANT\text{-}STEP} \quad = (50.1 - 0.2 \Delta\theta) \text{ spikes/sec}$$

$$\tau_{AG\text{-}AC} \quad = (11.7 - 0.2 \Delta\theta) \text{ msec}$$

$$\tau_{AG\text{-}DE} \quad = 0.2 \text{ msec}$$

$$\tau_{ANT\text{-}AC} \quad = 2.4 \text{ msec}$$

$$\tau_{ANT\text{-}DE} \quad = 1.9 \text{ msec}$$

$$c \quad = 0.0004 \text{ N-s/spike}$$

This then, is a complete description of the linear homeomorphic model for human eye movements and its evolutionary development. This development is traced in Table 1. Table 1 is not meant to be a summary of all good eye movement models. There are many more.[38, 54-60] However, these other models did not play a direct role in the evolution of the final model, so they are not included in the table.

III. TECHNIQUES FOR VALIDATING MODELS

Although everyone makes models, few people validate their models. One question

Table 1
EVOLUTION OF THE LINEAR HOMEOMORPHIC MODEL
FOR HUMAN EYE MOVEMENTS

Author	Innovation	Achievement
Descartes (1630)[5]	Concept of reciprocal innervation	First explicit model
Westheimer (1954)[6]	Linear, second-order model	Fit 10° saccades
Robinson (1964)[8]	Pulse-step input	Fit various size saccades
Cook and Stark (1968)[9]	Implementation of reciprocal innervation	Model velocity matches human
Clark and Stark (1974)[10]	Fine tuning of parameters	Model acceleration matches human
Collins (1975)[15]	Human physiological data	Clinical usage of a model
Bahill et al.[11,61]	Effects of controller signal, signal variations	Simulated eye movements not used in design of model, e.g., glissades and dynamic overshoot
Hsu et al. [12]	Sensitivity analysis	Method of validating model
Bahill[37,42]	Parameter estimation by function minimization, inclusion of length-tension diagram, sensitivity analysis	Linearized the model

which can be used to assess the validity of a model is, "Is the development of the model logical and scientific? First of all, the individual subsystems of the model must be valid. For example, the model of an agonist muscle must match data from physiological experiments on agonist muscles. A logical model development may produce valid subsystems. Each element of the newly developed linear homeomorphic eye movement model was based on a physiological experiment. Every experiment was explained and the sources of the data were presented. Most bioengineering models will pass this test for logical development.

Bahill et al.[62] used four other methods to validate their nonlinear reciprocal innervation model for human eye movements. First, they showed that position and velocity records of the model qualitatively matched those of humans. Second, they showed that the peak-velocity-magnitude-duration (main sequence) parameters of the model and humans matched over a range of 0.1 to 50° (Figure 2). Third, they used the model to simulate two novel eye movements that were not used in developing the model. They then made specific predictions about the neural signals responsible for these movements. Subsequent neurophysiological research confirmed these predictions for the phenomenon called dynamic overshoot. Their fourth validation technique was to perform a sensitivity analysis on the model parameters. Each parameter was varied and the effect on the peak velocity and magnitude was measured. In effect, the relative sensitivity function was evaluated once in the middle of the saccade and once near the end. The 18 parameters were then rank ordered.

Similarly, these four validation techniques were applied to this new linear model. There is a qualitative match between human and model outputs, as shown in Figure 13. Quantitatively, the mean squared error for a 10° saccade between human and model outputs is small. A type of eye movement that was not used in the construction of the model was simulated. When there is a mistake in constructing the pulse portion of the input controller signals, the eye will overshoot or undershoot the final eye posi-

$10.1°$ θ $10.5°$

$452°/s$ $\dot{\theta}$ $441°/s$

$31729°/s^2$ $25397°/s^2$

$\ddot{\theta}$

$24536°/s^2$ $29148°/s^2$

θ

$\dot{\theta}$

$\ddot{\theta}$
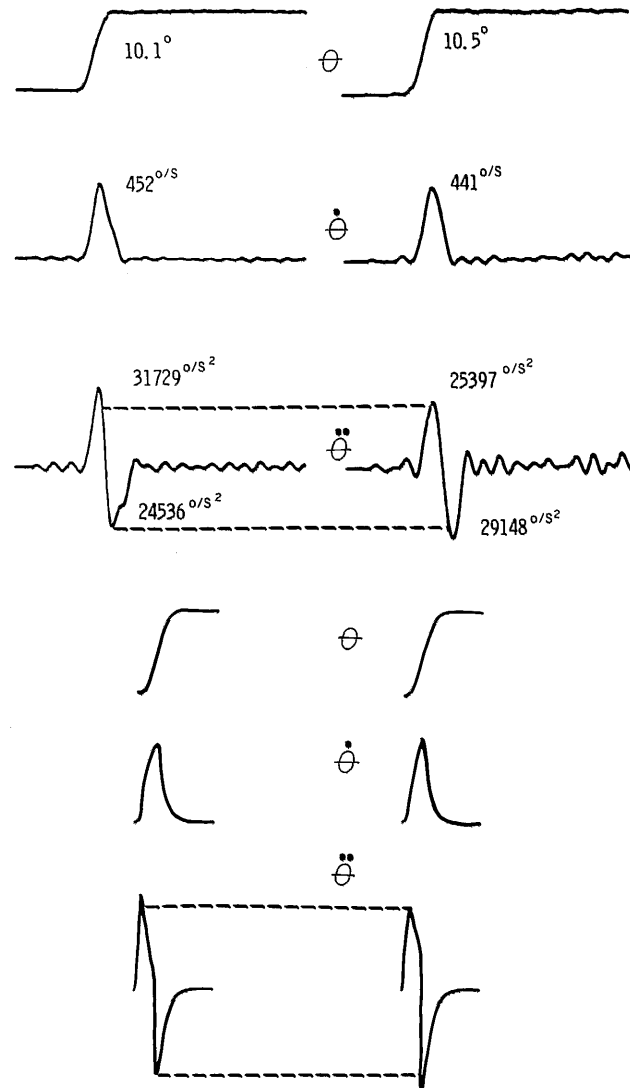
FIGURE 13. Model (bottom) and human (top) 10° saccadic eye movements with small differences between the simultaneous saccades of the right and left eyes. The left column (the left eye) and the right column (the right eye) show from top to bottom eye position, eye velocity and eye acceleration all as functions of time. The human records are 340 msec in duration. Differences between right and left eyes show up best in the acceleration traces. To match the right-eye left-eye differences in the human records, pulse width and pulse height were made to differ by 5% or less in the two model simulations.[85]

tion and then slowly drift to the final position. These drifts are called glissades. Simulations have led to the prediction that these glissadic overshoots and glissadic undershoots are due to pulse-width errors and not to pulse-height errors or a combination of pulse-height and pulse-width errors.[37] The sensitivity analysis[42] explained why pulse-width and not pulse-height errors are responsible for glissades. Furthermore, it helped to validate this linear model, by showing which parameters were most important and when they had their maximum effect on the output.

A. Minimization of Mean Squared Error

One of the reasons that the main sequence diagrams (Figure 2 and Reference 1) had so little scatter is that the eye position records were differentiated in a digital computer to yield eye velocity records. Then these eye velocity records were used to measure the duration and peak velocity of the saccades. Defining the duration to be the time between zero velocity at the start of the saccade and zero velocity at the end of the saccade gave a more accurate measure of duration than did any method using the eye position records. This then showed the advantage of using eye velocity traces to aid in human visual information processing.

Similarly, Cook and Stark[9] used a velocity trace (Figure 4) to point out the superiority of their model over Robinson's.[8] If the trick works once, why not try it twice? Hsu et al.[12] differentiated the eye position trace twice to get acceleration as a function of time. They spent many hours fine tuning their model to make the acceleration traces match the human data. The acceleration traces pointed out differences that were not visually apparent in the velocity or position traces (see Figure 13).

However, the acceleration and velocity records were derived from the position records, so all of the information must be contained in the position records. It may not be easy for a human to see the differences, but a computer certainly can. This prompted Bahill et al.[37] to do all of the matching and comparing with computer programs operating on the eye position records.

A numerical estimation of the difference between several models and a typical human saccadic eye movement was computed. The results are shown in Table 2. Each model was run for 60 msec. The resulting record was then compared point by point to the human saccadic eye movement, and the mean squared error was calculated. This process was repeated 50 times as the model was shifted forward and backward in time. The shift with the minimum mean squared error was chosen as the best possible fit for that model. The linear homeomorphic model[37] had the least mean squared error.

For the linear homeomorphic model the simulations match human eye movements better than the two eyes match each other. Biological variations (noise) produce larger differences in saccadic trajectories than those caused by small parameter adjustments. This implies that the model parameters have been selected optimally. Therefore, this is the best model for saccades in general. By using the parameter estimation routine the mean squared error can be made to approach zero for any particular saccade. Thus this model can be made exact for any particular saccade.

The time response of a linear second-order undamped system, such as Westheimers model,[6] to a step input of magnitude $\Delta\theta$ is

$$\theta(t) = k \, \Delta\theta \left[1 - \frac{e^{-\zeta\omega_n t}}{\sqrt{1-\zeta^2}} \sin(\Omega_n\sqrt{1-\zeta^2}\, t + \phi) \right] \qquad \phi = \text{Tan}^{-1} \frac{\sqrt{1-\zeta^2}}{\zeta}$$

This model can be made to fit human data if ω_n is allowed to be different for each saccade, (keeping $\zeta = 0.707$). The time to the first peak of the linear, second-order system is

$$T_p = \frac{\pi}{\omega_n\sqrt{1-\zeta^2}}$$

This must be set equal to the duration of a saccade.

$$DUR = (1.7 \, \Delta\theta + 20) \, \text{msec}$$

Table 2
MEAN SQUARED ERROR, IN DEGREES SQUARED × 10⁻⁶,
BETWEEN VARIOUS MODELS AND THE HUMAN 10°
SACCADIC EYE MOVEMENTS SHOWN IN FIGURE 13

Model	Error in matching left eye	Error in matching right eye	Ref.
Linear second-order, underdamped $\omega_n = 120$ rad/sec, $\zeta = 0.7$, step input	146	194	6
Unity, M(s) = θ_{rve}/input = 1	3501	3352	63,83
Linear second-order, overdamped $\tau_1 = 150$ msec, $\tau_2 = 12$ msec, with integrator and pulse input	2384	2640	56
Sixth-order nonlinear model without length-tension diagram	126	135	12
Sixth-order linear model without length-tension element	188	256	41
Sixth-order nonlinear model with length-tension element	45	75	85
Sixth-order linear model with length-tension element	49	66	37, Figure 11
Left eye of Figure 13	0	106	Figure 13
Right eye of Figure 13	106	0	Figure 13

Therefore

$$\omega_n = \frac{\pi\sqrt{2} \times 10^3}{1.7 \, \Delta\theta + 20}$$

This model does give a reasonable fit to the physiological data as shown in Table 2. The extreme simplicity of this model and the fact that it could be changed to match saccades of all sizes prompted Zuber et al.[60] to repropose this model in 1968.

Robinson's[56] model has a pulse input 50-msec wide and 20 $\Delta\theta$ high, where $\Delta\theta$ is the desired size of the saccade. (Subsequent versions of this model[54,55] have slightly different pulses.) The pulse passes through an integrator and a gain element and finally through a linear second-order overdamped plant. The transfer function for this saccade system is

$$\frac{\theta}{F} = \frac{0.15 \, s + 1}{s(0.15 \, s + 1) \, (0.012 \, s + 1)}$$

The response of such a system for the pulse input is

$$\theta(t) = \Delta\theta \, (20t + 0.24e^{-83t} - 0.24) \qquad \text{for } 0 < t < 0.05 \text{ sec}$$

$$\theta(t) = \Delta\theta \, (1 - 15e^{-83t}) \qquad \text{for } 0.05 \leq t$$

This model has a rather large mean squared error, 2500 degree²/sec for a 10° saccade. The performance of the model could be improved by making the width of the pulse depend upon the size of the saccade. For this model, the width of the pulse is about 70% of the duration of the saccade. So the pulse width could be 1.2 $\Delta\theta$ + 14 msec. The pulse height could be 1000 $\Delta\theta$/(1.2 $\Delta\theta$ + 14). Making this adjustment in pulse height and pulse width, this model had a mean squared error of 521 degree²/sec for a 10° saccade.

Another method used for evaluating a model is to use the model to simulate new types of eye movements; that is, to make predictions about the system. The linear homeomorphic model was used to make predictions about pathological patients and normal humans.

B. Predictions of the Model

A counter example of a model being able to make predictions is Westheimer's previously mentioned model. It was designed to simulate 20° saccades, but it could not simulate 30° saccades. It could not simulate novel movements not used in the construction of the model. Often the new phenomenon to be simulated is something that is well known, but ignored in the development of the model. Sometimes the new phenomenon is the result of a new discovery.

An eye movement has overshoot when the eye travels beyond its final position and then returns, finally coming to rest on the target. There are three distinct types of overshoot of saccadic eye movements: dynamic, glissadic, and static.[61] They are named according to their most distinctive feature, the behavior of the eye immediately after the primary saccade. Dynamic overshoot has a very fast saccadic return to the true target position. For example, the return phase of a 1° dynamic overshoot lasts about 20 msec and has a peak velocity of about 60°/sec. Glissadic overshoot has a slow gliding return phase which, for 1° of overshoot, lasts approximately 300 msec with a peak velocity of 5°/sec. In static overshoot the eye remains steady in the incorrect position for 150 to 200 msec until feedback instigates a corrective saccade, eliminating the error. Dynamic overshoot was a new discovery that was used to test the model. Glissadic overshoot was a previously known phenomenon that was ignored in the development of the model. It was also used to test the model. Static overshoot, because of its simplicity, could not be used to test the model.

1. Dynamic Overshoot

Dynamic overshoot (shown in Figure 14) is the most common type of saccadic overshoot. Two thirds of human saccades have dynamic overshoot. However, this varies greatly from subject to subject.[11] Dynamic overshoots are seldom shown in published eye-movement records because most published data have been low-pass filtered in order to remove noise. This removes the evidence of the dynamic overshoot. Therefore, the existence of dynamic overshoot was somewhat of a recent discovery.

Studies of the peak velocity-magnitude-duration relationships (main sequence diagrams) for normal saccades and for the return phases of dynamic overshoots suggested that the return phases of dynamic overshoots were small saccades. The peak velocity vs. magnitude main sequence diagram showed that the return phases of dynamic overshoots were just as fast as normal saccades and that both of these were much faster than vergence eye movements.[11]

Because the return phases of dynamic overshoots had saccadic dynamics, they were expected to have saccadic motoneuronal controller signals. To investigate this possibility, saccades with dynamic overshoots were simulated on the reciprocal innervation model. Dynamic overshoots were not used in the formulation of the model, so this served as an important test for the model.

A simulated saccade with dynamic overshoot is illustrated in Figure 14. This figure shows the eye position, eye velocity, active state tensions of the agonist and antagonist muscles, the motoneuronal signals required for the agonist and antagonist in order to produce dynamic overshoot, and finally the firing pattern of typical agonist and antagonist motoneurons. The reversal of motoneuronal activity at the end of the main pulse requires a high degree of synchronization between the motonuclei. For instance, the
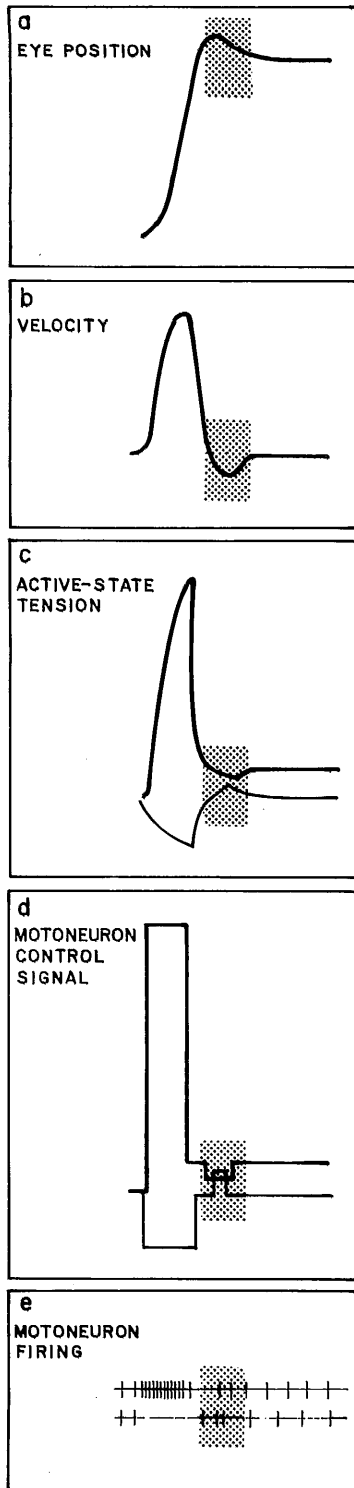
FIGURE 14. Position, velocity active-state tensions, controller signals, and firing of typical motoneurons for a saccade with dynamic overshoot. The return phase of this eye movement is a small saccade with pulse-step controller signals. (From Bahill, A. T. and Stark, L., *The Trajectories of Saccadic Eye Movements,* Copyright 1979, Scientific American, Inc. All rights reserved. With permission.)

firing rate of the pool of motoneurons supplying the agonist muscle rises from the original level to the high-frequency level, remains there until about the middle of the saccade, drops to a very low value, and then rises again up to its new step level. The pool of motoneurons innervating the antagonist muscle perform an analogous, but opposite task. Because of this motoneuronal innervation, the active state tensions of the muscles reverse. The active state tension of the agonist first becomes larger, then smaller, and then equal to all of its opposing forces. Dynamic overshoots must be caused by motoneuronal control signals reversals. However, these control signal reversals cannot be due to random noise because as many as a dozen consecutive saccades can have identical overshoot.

The modeling results enabled a prediction to be made that there should be pauses for the agonist motoneurons and bursts for the antagonist motoneurons in saccades with dynamic overshoot. Such pausing and bursting behavior could not easily be found in the neurophysiological literature. Once the prediction was made, investigators specifically looked for such behavior and found it in single-cell recordings of the brain stem of monkeys[64] and in human electromyographic recordings.[65]

Thus, the model was able to simulate a type of movement that as not known when the model was designed. Furthermore, predictions were made based on the modeling results, and these predictions were subsequently confirmed by neurophysiological experiments.

2. Glissades

Glissades are the slow gliding eye movements that are often appended to the end of normal human saccadic eye movements. Their frequency of occurrence is increased by fatigue and pathology.

Several papers[66-70] have suggested that the existence of glissades could be used to diagnose internuclear ophthalmoplegia, a syndrome that is usually caused by multiple sclerosis. In these patients there is a glissadic undershooting of the adducting eye and a concommitant overshooting of the abducting eye. There may also be abduction nystagmus.

The model was not built to simulate these glissadic eye movements; therefore, Bahill et al.[61] tried producing glissades in the model in order to test it and to try to understand the CNS errors which produce glissades. It was found that glissades could be caused by errors in either the pulse or the step components of the motoneuronal controller signal. Bahill et al.[71] continued these studies and only considered those glissades caused by errors in the pulse component. If the pulse was too small for its accompanying step, then the result was glissadic undershoot, as shown in Figure 15d and on the left in Figure 16. If the pulse was too large for the accompanying step, then glissadic overshoot would result, as shown in Figure 15c and on the right in Figure 16. They[71] further limited their study by considering only glissadic overshoot.

There are two ways of making the pulse portion of the motoneuronal controller signal too large, thereby mismatching the pulse and step components of the controller signal. The pulse could be either too wide or too high. Both of these possibilities were tried in the model. The resulting mismatched saccades had similar qualitative shapes, but different quantitative main sequence parameters. The saccade with a glissade appended created by a pulse-height error had a larger than normal peak velocity. The saccade with a glissade appended created by a pulse-width error had approximately normal peak velocity. Therefore, based upon this model behavior, a prediction was made. It was predicted that saccades with glissades appended to them would have abnormally high or slightly low peak velocities.

After the modeling studies were completed, human physiological data were gathered to test this prediction. It was found that human saccades with glissadic overshoot actually had slightly low peak velocities.[71]
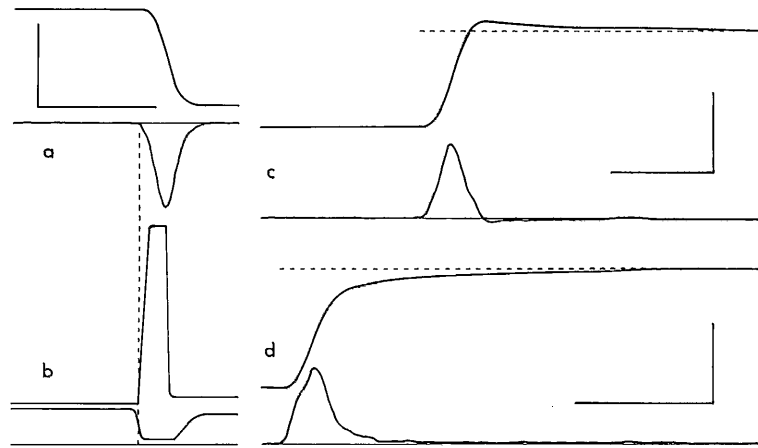
FIGURE 15.   Three types of glissadic behavior. Eye position and eye velocity as
functions of time for saccadic eye movements with no glissade (a), glissadic over-
shoot (c), and glissadic undershoot (d). The hypothesized firing frequencies for the
agonist (top) and the antagonist (bottom) motoneuronal pools are shown in (b).
The calibrations represent 13° and 640°/sec (a), 14.6° and 600°/sec (c), and 10°
and 500°/sec (d). The time calibration in each represent. 100 msec. No time delay
is shown between onset of motoneuronal activity and the start of saccade because
this delay is not fixed. It depends upon where the motoneuronal activity is meas-
ured. (From Bahill, A. T., Clark, M. R., and Stark, L., *Math. Biosci.*, 26, 303,
1978. Copyright Elsevier North-Holland, Inc. With permission.)

Bahill et al.[37] applied the parameter estimation routine to the model to study glis-
sades. The glissadic undershoot, illustrated in the left colum of Figure 16, could be
matched with minimum mean squared error only if the pulse width were reduced by a
large amount. When the parameter estimation routine was allowed to vary pulse width
and pulse height the only two physiological parameters that are likely to change be-
tween saccades, to fit the data, the best fit was obtained by changing the pulse width
by 20% and the pulse height by 2%. Similarly, the overshoot in the right column of
Figure 16 could be matched with minimum mean squared error only if the pulse width
were increased by a large amount (25%).

This result confirms that *glissadic overshoot* in normal humans is caused by pulse-
width errors. Furthermore, it also showed that *glissadic undershoots* are caused by
pulse-width errors and not pulse-height errors. Using the parameter estimation routine
to make these conclusions was much simpler than the previous method.[71] Furthermore,
it also ruled out a combination of pulse-width and pulse-height errors as the cause of
glissades. These results implied that CNS mechanisms can control the height of a mo-
toneuronal burst quite accurately, but it is more difficult to control the duration of a
motoneuronal burst.

This implies that in normal eye movements in which glissadic overshoot is the result
of a too-large pulse, the error is caused primarily by the brain's mistake in computing
the pulse width, not the pulse height. This, in turn, implies that normal human glis-
sades are not caused by peripheral disturbances, but are caused by the CNS networks
that produce the pulse width. It also implies that in controlling a neuronal burst, it is
easier for the CNS to regulate pulse height than pulse width. Perhaps this is because
pulse height control is hardwired (*a la* the Henneman size principle).

3. Other Predictions

When humans fatigue they often use two small saccades rather than one large sac-
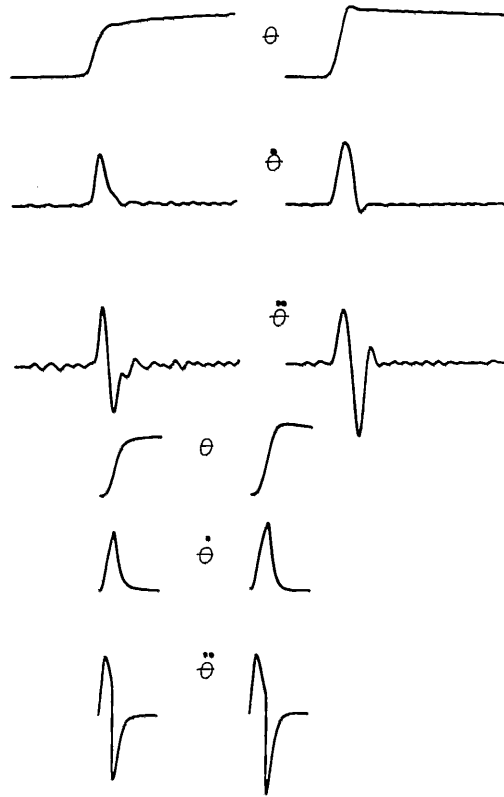
FIGURE 16.   Model (bottom) and human (top) 10°
saccadic eye movements with large differences between
two sequential saccades of the left eye. Large differ-
ences such as these are caused by control signal varia-
tions. To produce similar model saccades, with minimal
mean squared error between model and human sac-
cades, the pulse width had to be decreased by 20% to
produce the glissadic undershoot in the left column, and
the pulse width had to be increased by 25% to produce
the overshoot in the right column. In both cases the
pulse height had to be held within 2% of the nominal
value. Plotting parameters are the same as in Figure
13.[85]

cade to execute a change of fixation. [72] Often the velocity profiles of these saccades
overlap. The underlying motoneuronal control signal for these overlapping saccades
could not be described when they were first discovered. It was only with the aid of the
model that the controller signals could be demonstrated.

The model showed that the pulse width of the motoneuronal controller signal was
only about half the duration of the saccade.[73] Therefore, two saccades could overlap
without having their control signals overlap.

How does the brain code or control the size of a saccade? For small saccades it
seems to be pulse-height control, for large saccades pulse-width control, and for me-
dium-sized saccades a combination of both.[12] There are two lines of thought that led
to these conclusions.

First, the main sequence diagrams (Figure 2) can be divided into three regions judg-
ing from the slopes of the curves: the first region for saccades smaller than 1°, the

second for saccades greater than 10°, and the third for saccades in between 1 and 10°. The duration of a saccade is strongly correlated with the duration of the high-frequency burst of oculomotoneuronal firing (PW). We see that large amplitude saccades show a strong dependence on pulse width since the main sequence has the greatest slope for large saccades. Small-magnitude saccades seem to be controlled only by pulse height since the main sequence duration plot shows a scattergram rather than a tight cluster of points. The region in between 1 and 10° saccades seems to be controlled by both pulse width and pulse height.

The second collaborating fact comes from the model equations. The values of pulse height (PH) that minimized the mean squared error between the human and model data were best fit with two straight lines intersectins at 10°. Above 10° the slope was very small, showing little control of saccadic magnitude by pulse height. Below 10° the slope was large, showing pulse-height control of saccadic magnitude. The pulse-width equation is

$$PW_{AG} = (10 + \Delta \theta) \text{ msec}$$

Variations of saccadic magnitude ($\Delta \theta$) will not produce large changes in pulse width for saccades of 1° and less. Therefore pulse height would be the only controlling parameter for saccades 1 ° and smaller.

Thus, a prediction based on the model and on the main sequence diagrams is that the brain uses pulse-width control for large saccades, pulse-height control for small saccades, and a combination of pulse-height and pulse-width control for medium-sized saccades.

C. Sensitivity Analysis

Sensitivity analyses are an important method of validating economic models,[74] societal models,[75] engineering models,[76] and physiological models.[12,42,38]

A sensitivity analysis shows how a model's outputs change with variations in the model parameters. The sensitivity analysis may be analytic or experimental. The results of a sensitivity analysis can be used (1) to validate a model, (2) to warm of strange or unrealistic model behavior, (3) to suggest new experiments or guide future data collection efforts, (4) to point out important assumptions of the model, (5) to guide the formulation of the structure of the model, pointing out which unimportant elements can be treated simply, and (6) to help select numerical values for the parameters. The sensitivity analysis tells which parameters are the most important and most likely to affect predictions of the model. Values of critical parameters can then be refined, while parameters that have little effect can be simplified or ignored.

If the sensitivity functions are calculated as functions of time, then it can be seen when each parameter has its greatest effect on the output function of interest. This can be used to select numerical values for the parameters. The values of the parameters will be chosen to match the physiological data at the times when they have the most effect upon the output. Sensitivity analyses can also be used to suggest future experiments to elucidate biological systems.

A traditional root-locus plot graphically displays the results of a sensitivity analysis: it shows the movement of the systems closed-loop poles as a function of the system gain. This technique can be generalized to show the movement of the systems closed-loop poles as each parameter of the model is varied.[35,38] There are canned computer programs for this type of sensitivity analysis.[77]

A partial derivative is a sensitivity function. For example, in a system described by

analytic functions, calculating partial derivatives constitutes a sensitivity analysis. There are several common definitions for sensitivity functions. Three commonly used functions are absolute sensitivity, relative sensitivity, and semirelative sensitivity.[76]

The *absolute sensitivity* of the function F (which is a function of alpha and time) to variations in the parameter α, evaluated at the nominal parameter value α_o, is given by

$$S_\alpha^F = \frac{\partial F}{\partial \alpha}\bigg|_{\alpha_o}$$

Absolute sensitivity functions are useful for calculating output errors due to parameter variations and for assessing the times at which a parameter has its greatest or least effect.[76]

The *relative sensitivity* of the function F to the parameter α evaluated at the nominal value of that parameter is given by

$$\bar{S}_\alpha^F = \frac{\partial \ln F}{\partial \ln \alpha}\bigg|_{\alpha_o} \qquad \bar{S}_\alpha^F = \frac{\partial F/F}{\partial \alpha/\alpha}\bigg|_{\alpha_o} = \frac{\partial F}{\partial \alpha}\bigg|_{\alpha_o} \frac{\alpha_o}{F_o}$$

Relative sensitivity functions are ideal for comparing parameters because they are dimensionless, normalized functions.

Both of these sensitivity functions are evaluated at the operating point where the parameters take on their nominal values. Both of these sensitivity functions are functions of time.

Because the old reciprocal innervation model was a sixth-order nonlinear model, the analytic partial derivative technique for sensitivity analysis was not feasible. An empirical sensitivity analysis was performed by Hsu et al.[12] for a 10° saccade because this was a normal physiological magnitude and data were both abundant and relatively noise free. Each parameter was varied from 20 to 200% of the value used for producing a good 10° saccade, while the other 19 parameters were held constant. Figure 17 shows examples of trajectory variations produced when pulse width and pulse height were varied. These simulations were the method used to numerically estimate the partial derivatives of the eye position and the eye velocity with respect to each of the parameters. The sensitivity of eye position with respect to each parameter was evaluated for one instant of time near the end of the saccade; the sensitivity of eye velocity was evaluated near the middle of the saccade. These were plotted as functions of each parameter. The slopes of these sensitivity curves gave a measure of the relative importance of each parameter. The steeper the slope, the more eye movement behavior changes were produced by variation of that parameter. For instance, when the pulse width was 20 msec, the saccadic magnitude was 10°. When pulse width was doubled to 40 msec, the saccadic magnitude became 17.3°, increasing by 73%. However, when another parameter, the series elasticity of the agonist, was doubled (from 1.8 to 3.6 g tension/°), the saccadic magnitude increased by only 7%. The slope of the magnitude sensitivity curve for pulse width was 0.54 compared to 0.1 for series elasticity of the agonist. This sensitivity analysis showed which parameters had the greatest effects on the model. When the parameters did not describe the input controller signals, several sources of good physiological data had to be found to justify the parameter values.

This nonlinear model was most sensitive to four parameters: pulse width, pulse height, the agonist dashpot (B_{AG}), and the parallel elasticity (K_P). These parameters are similar to those defined in Figure 1. Pulse width and pulse height described the
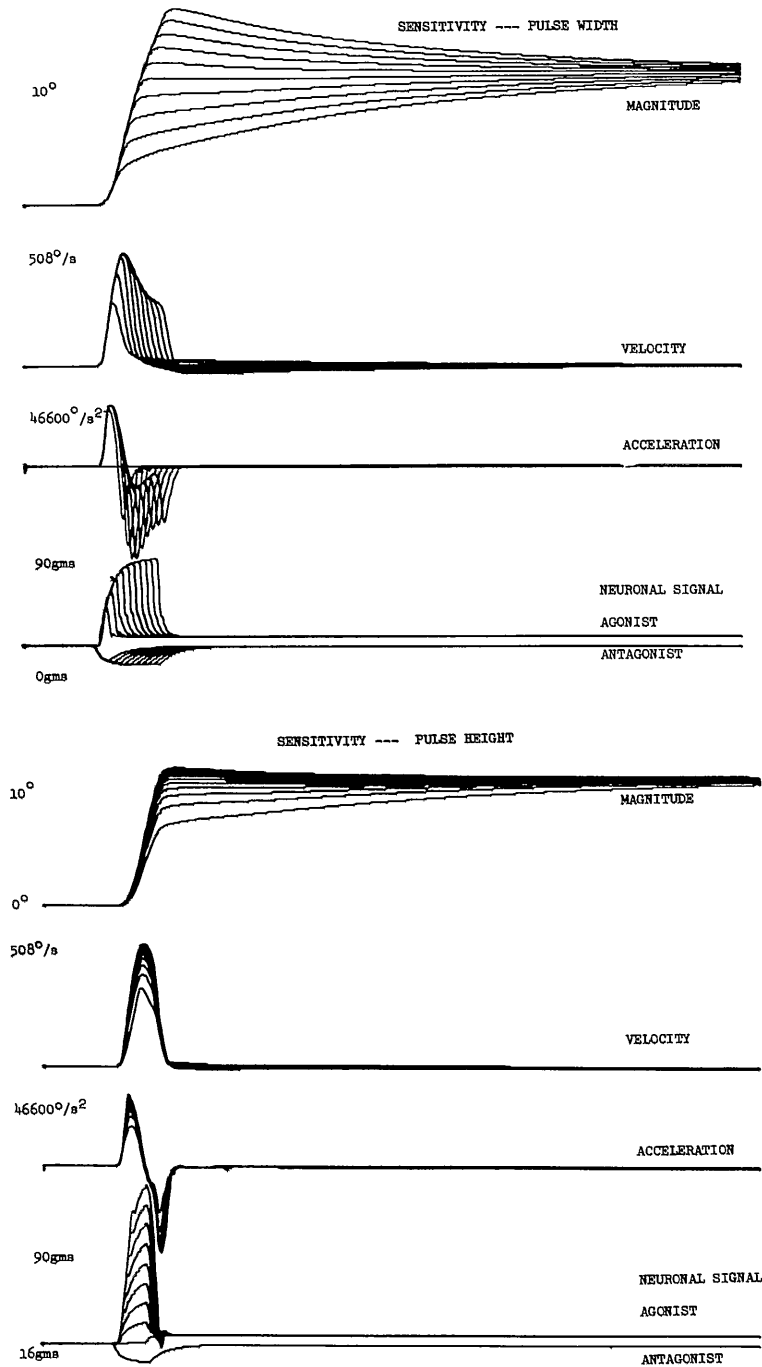
FIGURE 17. Trajectories of position, velocity, acceleration, and active state tensions as pulse width (PW) (a), and pulse height (PH) (b) were varied from 20 to 200% of the value used for producing a good 10° saccade. Varying pulse width had a large effect on the magnitude of saccades but a small effect on peak velocity. The shapes of the velocity and acceleration trajectories are drastically changed nevertheless. Varying pulse height affects all trajectories as shown. Record length is 500 msec. (From Hsu, F. K., Bahill, A. T., and Stark, L., *Comput. Programs Biomed.*, 6, 108, 1976. With permission.)

input control signals. Therefore, it was reasonable for the model to be sensitive to their variations. K_p was a large, lumped parameter, and there was ample physiological data for the calculation of its value. Therefore, it was neither surprising nor disturbing that the model was so sensitive to its variations. However, the sensitivity of the model to B_{AG}, the agonist apparent viscosity, was disturbing. B_{AG} is a constant in the Hill equation for the force-velocity relationship of muscle. It is related to the maximum muscle velocity (V_{max}), which is different for different muscles. Data for this parameter had been extrapolated from cat data. Because the model was so sensitive to B_{AG}, experiments were performed to investigate it in greater detail. The treatment of this agonist dashpot was revised in subsequent models.

In contrast, the model behavior had very little dependence on many other parameters. For instance, the sensitivity of the output to variations of the inertia, J, was almost zero. This then was the justification for modeling the inertia of the eye ball as a globe of ice rather than as a series of concentric shells connected with visco-elastic elements. The sensitivity analysis provided direct information concerning the importance of each parameter, helped choose numerical values for the parameters, and suggested new experiments for further understanding of the system and for updating the model.

Sensitivity functions are usually functions of time. In the preceding analysis the sensitivity functions were evaluated at only two points in time: near the middle and near the end of the saccade. However, the analysis covered a broad range of parameter pertubation sizes: from 20 to 200% of the nominal values. If one parameter pertubation size is sufficient, as is the case with a linear system, then it may be advantageous to look at sensitivity as a function of time.

The absolute sensitivity function, $S = \partial y / \partial \beta$, where y is the output and β is the parameter of interest, is useful for computing parameter-induced output errors, but is not useful for comparing effects of different parameters.[76] For this comparison we want a relative sensitivity function such as

$$\bar{S} = \frac{\partial \ln y}{\partial \ln \beta} = \frac{\partial y}{\partial \beta} \frac{\beta_0}{y_0}$$

where β_0 and y_0 are the values of β and y at the nominal operating point. However, for a 10° saccadic eye movement the nominal output value, y_0, varies from 0 to 10° and division by zero is frowned upon. Furthermore, the relative sensitivity function emphasizes the beginning of the saccade where y_0 is small. In contrast, the semirelative sensitivity function

$$\tilde{S} = \frac{\partial y}{\partial \ln \beta} = \frac{\partial y}{\partial \beta} \beta_0$$

weights the sensitivity evenly throughout the saccade. Therefore, the semirelative sensitivity function was used by Bahill et al.[42] The semirelative sensitivity function is the best choice when the function of interest is a function of time, such as a step response or an impulse response.

For a linear system with small parameter changes the semirelative sensitivity function becomes

$$\tilde{S} = \frac{\Delta y}{\Delta \beta} \beta_0$$
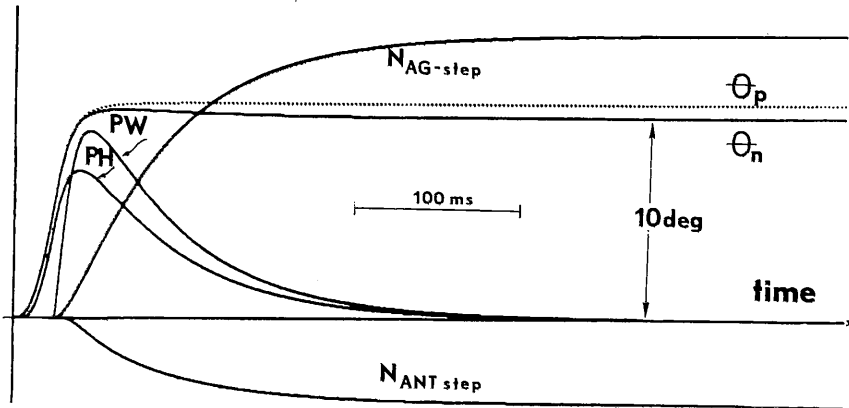
FIGURE 18.   Nominal (solid line labeled θ_n) and perturbed (dotted line labeled θ_p) 10° saccadic eye movements and the semirelative sensitivity functions for the parameters describing the input controller signals. Record length is 490 msec. The pulse width (PW) and pulse height (PH) primarily affect the dynamic saccade and the behavior immediately following. The steady-state neural firing levels, $N_{AG-step}$ and $N_{ANT-step}$, primarily affect the static behavior of the eye. The effect of $N_{ANT-pulse}$ is too small to be seen on this scale. Its sensitivity function looks like noise on the abscissa. The perturbed saccade is that produced by increasing $N_{AG-step}$ by 5%. Eye position and the semirelative sensitivity functions have the same units, degrees, and are plotted to the same scale. (From Bahill, A. T., Latimer, J. R., and Troost, B. T., *IEEE Trans. Syst. Man Cybern.*, SMC-10, December 1980. With permission.)

To perform the sensitivity analysis, a 10° saccade was simulated (solid line labeled θ_n in Figure 18).[42] Then one parameter was changed by a set amount, +5% for these figures, and the model was run again producing the preturbed saccade (dotted line labeled θ_p in Figure 18). The difference between the nominal and preturbed saccades (Δy) was calculated for each millisecond and this difference was divided by the change in the parameter value ($\Delta \beta$). This ratio was then multiplied by the nominal parameter value (β_0). This process was repeated for each of the 18 parameters in the model. The results are the sensitivity functions of Figures 18 and 19. The model was most sensitive to the input control signals for the agonist muscle, $N_{AG-step}$, PH and PW. The control signals for the antagonist, $N_{ANT-step}$ and $N_{ANT-pulse}$ were not as important.

Some of the parameters affected the dynamic properties of the saccade and some parameters affected primarily the steady state or static behavior, the behavior after the dynamic saccade was over. Five of the sensitivity functions of this study were monotonic, like the sensitivity to $N_{AG-step}$. Most sensitivity functions were monophasic. The sensitivity for the inertia, J, was the only biphasic function. Sensitivity of K_{ANT-SE} was the only function with a relative minimum as well as different absolute minimum.

Table 3 compares the maximum values of the 18 sensitivity functions. The first column is a rank ordering of the maximum values of the semirelative sensitivity functions of all 18 parameters of the linear model. This table also compares the results of two other sensitivity analyses of similar models.

The comparisons shown in Table 3 are not strictly parallel. The ranking of Bahill et al.[42] was based on the maximum value of the semirelative sensitivity function, whereas the other rankings were based on the relative sensitivity function evaluated near the middle of the saccade where the peak velocity occurred. Hsu et al.[12] had two constants for each dashpot, and the sensitivity ranking of both of these coefficients is listed in this table. NA means the element was not included in the model or else the parameter was not included in the sensitivity analysis. The elements with rank 12 and 14 in the Hsu et al. sensitivity analysis were the amount of time by which the antagonist pre-
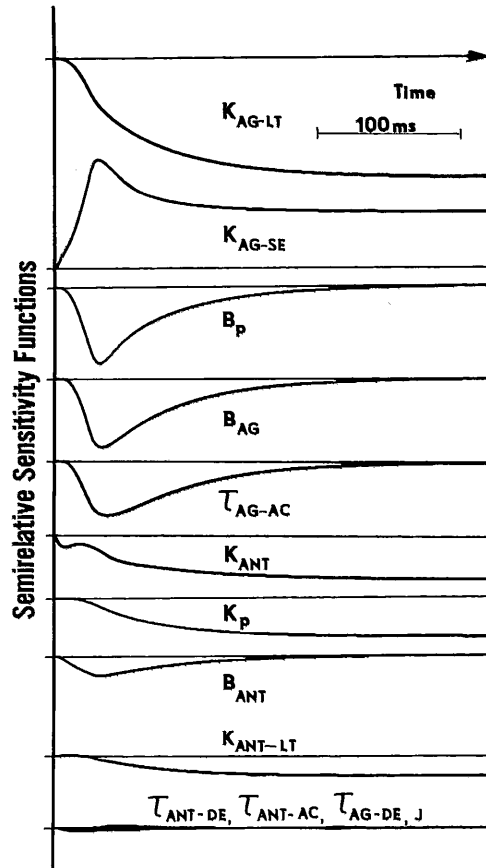
FIGURE 19.   Semirelative sensitivity functions for
the other 13 parameters of the model. The functions
for J, τ_{ANT-AC}, τ_{AG-DE}, and τ_{ANT-DE} overlap each other
and are not distinct on this scale. The curve for the
antagonist series elasticity is labeled K_{ANT}. (From
Bahill, A. T., Latimer, J. R., and Troost, B. T.,
IEEE Trans. Syst. Man Cybern., SMC-10, Decem-
ber 1980. With permission.)

ceded and succeeded the agonist pulse. Because the parameters had so little effect, they
were treated as fixed constants in the later models. Lehman and Stark[38] used only one
parameter to describe the agonist and antagonist activation-time constants. In the table
they were treated as two constants. The deactivation time constants and the series
elasticities were treated similarly.

The following conclusions were derived from the Bahill et al.[42] sensitivity analysis.

1.   The series elasticity of the agonist, K_{AG-SE}, is the only parameter that has an im-
portant effect on both static and dynamic properties.
2.   The parameters $N_{AG-step}$, $N_{ANT-step}$, K_{LT}, and K_p affect the steady state of $\theta(t)$ and
3.   The sensitivity functions for the time constants are very small.
4.   The sensitivity functions for three of the time constants and for the three dash-
pots had shapes that were similar to each other and that peaked near the end of
the saccade. This means that trade offs could be made between these six param-
eters without affecting the precision of the model.

Table 3
RANK ORDERING OF SENSITIVITY FUNCTIONS
FOR VARIOUS RECIPROCAL INNERVATION
MODELS

	Bahill et al.[42]	Hsu et al.[12]	Lehman and Stark[38]
$N_{AG\text{-}step}$	1	NA	NA
PW	2	1	3
$PH = N_{AG\text{-}pulse}$	3	2	1
$K_{AG\text{-}LT}$	4	NA	NA
$K_{AG\text{-}SE}$	5	10	6
B_P	6	16	9
$N_{ANT\text{-}step}$	7	NA	NA
B_{AG}	8	3,8	2
$\tau_{AG\text{-}AC}$	9	7	4
$K_{ANT\text{-}SE}$	10	17	7
K_P	11	4	8
B_{ANT}	12	5,6	10
$K_{ANT\text{-}LT}$	13	NA	NA
$\tau_{ANT\text{-}DE}$	14	11	11
J	15	15	13
$\tau_{ANT\text{-}AC}$	16	13	5
$N_{ANT\text{-}pulse}$	17	18	NA
$\tau_{AG\text{-}DE}$	18	9	12

5. Pulse height (PH) and pulse width (PW) primarily affect the output near the end
    of the saccade and immediately following the saccade. Variations in both of these
    parameters produce slow drifts after the saccades. These drifts are called *glis-
    sades*. However, the shapes of these two sensitivity functions differ. The pulse-
    height function rises gradually, starting at the beginning of the saccade, whereas
    the pulse-width sensitivity function is zero until near the end of the saccade,
    where it abruptly rises to its peak, as shown in Figure 18. This means that increas-
    ing either parameter would produce a larger saccade with a glissade attached to
    the end. However, increasing the pulse height would also increase the peak veloc-
    ity of the saccade, whereas increasing the pulse width would not affect the peak
    velocity, because the peak velocity occurs in the middle of the saccade while this
    sensitivity function is still zero. Physiological data have shown that saccades with
    this type of glissade appended have normal or even lower than normal peak ve-
    locities.[71] Therefore, the sensitivity analysis explains why glissades are caused by
    pulse-width not pulse-height errors. Early studies of glissades[78,61] suggested that
    glissades could be caused by pulse-width or pulse-height errors. This sensitivity
    analysis clearly showed that this is not so.

Because the sensitivity functions were functions of time, it was easy to see what part
of the movement should be studied in order to see the effects of any particular param-
eter. For example, the time constant $\tau_{ANT\text{-}DE}$ has its greatest effect on the output early
in the saccade. Thus if you wish to study this parameter, you should study the begin-
ning of the saccade. If your study involves visual inspection of the waveforms, you
might use the models output to derive some other function that will highlight this
region, such as the acceleration as a function of time. Then to study the effects of $\tau_{ANT\text{-}DE}$ you would look at the peak positive acceleration. A similar study of derived param-
eters was performed by Lehman and Stark[38] on their model.

Another reason for using relative or semirelative sensitivity functions rather than an

absolute sensitivity function is that the former will not change their values depending upon the units used to describe the parameters. For example, the maximum value of the semirelative sensitivity of eye position with respect to pulse height is 7.1°, whereas the maximum value of the absolute sensitivity of eye position with respect to pulse height is 0.043°/g if the pulse height is given in units of grams-tension. It is 4.39°/N if the pulse height is given with units of newtons.

For the most part, this rank ordering of the sensitivity functions was similar to the results of Hsu et al.[12] and Lehman and Stark[38] (see Table 3). The only exception was the sensitivity to B_{AG}. In the analysis of Bahill et al.[42] it ranked eighth. In the other studies it ranked second or third. Because human physiological data are not available for this parameter, Bahill et al.[42] felt that it was good that the parameter did not play an important role in their model.

This model is neither the simplest nor the most complicated possible model for a sixth-order system. In general, a sixth-order system can be described with a gain parameter and a characteristic polynominal containing only six coefficients or with a six by six A matrix with 36 coefficients. This linear model contains 18 parameters. Using sparce matrix techniques, this model could be condensed to 12 A-matrix entries. However, the model should not be condensed, because each element of the model corresponds to a real element or effect in the physiological system; the model is homeomorphic. Homeomorphism makes it possible to use the model to explain which human parameters might have been changed by pathology, fatigue, or drugs to produce certain abnormal human eye movements.[79]

D. Validation Summary

Physiological data were used to build a linear homeomorphic reciprocal innervation model for the eye movement system. The model was validated qualitatively by comparing shapes of human and model saccades, quantitatively by comparing main sequence relationships of human and model saccades, quantitatively by computing the mean squared error between the model output and the human response, analytically by performing a sensitivity analysis, and heuristically by simulating eye movements that the model was not designed to simulate. Use of the model enabled the following predictions to be made

1. Dynamic overshoots are caused by reversals in the neurological control signals (based on the nonlinear model[12]).

2. When there are glissadic overshoots or undershoots, with the eye drifting (or glissading) onto the final target position, there was an error made in computing the pulse width and not the pulse height of the motoneuronal controller signal.[37]

The first prediction has been subsequently confirmed in physiological studies.

The validation of this model was presented as an example of model validation. There were five major components of this validation scheme: logical development, qualitative comparisons, quantitative comparisons, simulation of data not used in the model formulation, and the sensitivity analysis. These techniques were all helpful in validating the model.

IV. DENOUEMENT

The sixth-order, linear, homeomorphic model whose development and validation has just been presented is but one small part of the overall closed-loop eye-position control system. Figure 20, based on References 7, 63, and 80 to 84, shows a model for the whole system. It includes two types of adaptive control.

Adaptive Gain Controller

Saccadic Branch

Target Position

+

Dead Zone   Sampler   Delay   Integrator   Zero Order Hold   Gain

$\frac{1}{Z}$ $\frac{Z}{Z-1}$ $\frac{1-e^{-st}}{s}$ G

Time Optimal Controller

±   +

Reciprocal Innervation Plant

Eye Position

Smooth Pursuit Branch

Differentiator

+   +   S

Limiter   Control Loop Integrator   Saturation   Delay   Velocity to Position Integrator

$\frac{1}{s}$ e^{-st} $\frac{1}{s}$

Internal Model

H

Bahill 1980
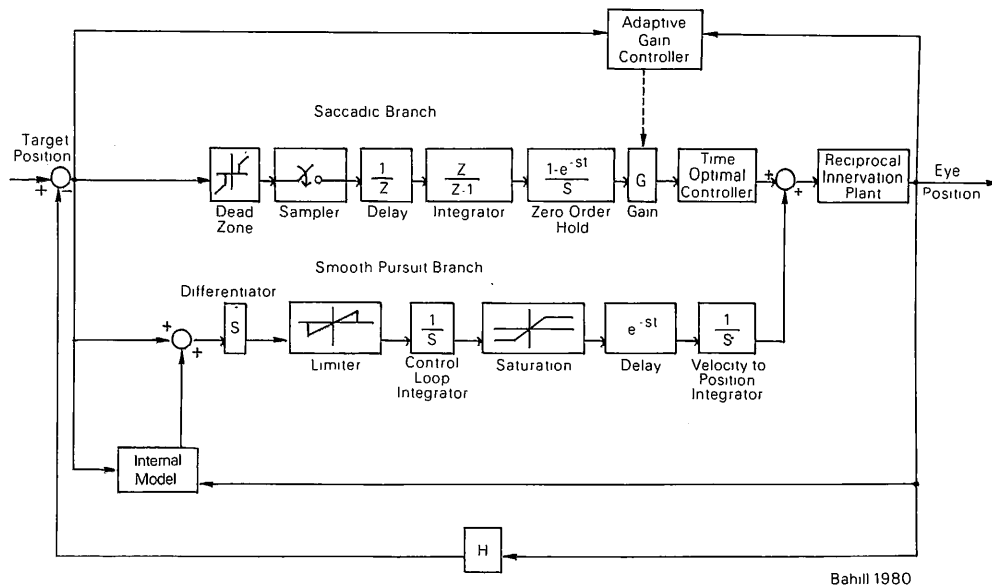
FIGURE 20. Ocular motor tracking system, including the saccadic branch, the smooth-pursuit branch, and the adaptive control processes. An internal, adaptive model for the target movement is used for smooth-pursuit tracking of predictable targets motions. The gain of the saccadic system is adaptively controlled by the cerebellum. The feedback element, H, is normally unity.

The cerebellum is probably the adaptive controller for the saccadic eye movement system. It receives inputs from the visual, vestibular, and proprioceptive sensory systems and sends outputs to the oculomotor system. It is hypothesized that the cerebellum monitors the input signals from the sensory systems and also monitors the resulting output of the oculomotor system. If they differ, then the cerebellum exerts its adaptive control capabilities and changes the gain of the saccadic controller.[63]

The smooth pursuit system also shows evidence of adaptive control. When humans track periodic targets, they very quickly lock onto the target movement and are able to track it with no latency. It is as if they create an internal (or CNS) model of the target movement and then track the output of this model, rather than the actual visual target. This internal model has variously been called a state estimator, an observer, a long-term learning process, a percept tracker, a predictor, and an adaptive controller.[84] This internal model is a part of the overall tracking system, but it is an additional component that was eliminated in earlier studies.[30] After the fundamental smooth pursuit system was adequately modeled, this internal model (or adaptive control function) could be incorporated into the model of Figure 20.

The logical extension of the research summarized in this review paper is to apply the validation techniques shown here to the overall, closed-loop control system model for the human eye position system of Figure 20.

REFERENCES

1. Bahill, A. T. and Stark, L., The trajectories of saccadic eye movements, *Sci. Am.*, 240(1), 108, 1979.
2. Javal, E., Essai sur la physiologie de la lecture, *Ann. Ocul.*, 82, 242, 1879.
3. Stark, L., Kong, R., Schwartz, S., Hendry, D., and Bridgeman, B., Saccadic suppression of image displacement, *Vision Res.*, 16, 1185, 1976.
4. Campbell, F. W. and Wurtz, R. H., Saccadic omission! Why we do not see a gray-out during saccadic eye movement, *Vision Res.*, 18, 1297, 1978.
5. Descartes, R., *Treatise of Man,* originally published by Charles Angot, Paris, 1664; published with translation and commentary by Hall, T. S., Harvard University Press, Cambridge, 1972, 20.
6. Westheimer, G., Mechanism of saccadic eye movements, *Arch. Opthamol.*, 52, 710, 1954.
7. Young, L. R. and Stark, L., Variable feedback experiments testing a sampled data model for eye tracking movements, *IEEE Trans. Hum. Factors Electron.*, HFE-4, 38, 1963.
8. Robinson, D. A., The mechanics of human saccadic eye movement, *J. Physiol.*, 174, 245, 1964.
9. Cook, G. and Stark, L., The human eye movement mechanism: experiments, modeling and model testing, *Arch. Opthalmol.*, 79, 428, 1968.
10. Clark, M. R. and Stark, L., Control of human eye movements, *Math. Biosci.*, 20, 191, 1974.
11. Bahill, A. T., Clark, M. R., and Stark, L., Dynamic overshoot in saccadic eye movements is caused by neurological control signal reversals, *Exp. Neurol.*, 48, 107, 1975.
12. Hsu, F. K., Bahill, A. T., and Stark, L., Parametric sensitivity of a homeomorphic model for saccadic and vergence eye movements, *Comput. Programs Biomed.*, 6, 108, 1976.
13. Bahill, A. T., *Bioengineering: Biomedical, Medical and Clinical Engineering,* Prentice-Hall, Englewood Cliffs, N. J. 1981.
14. Robinson, D. A., OMeara, D. M., Scott, A. B., and Collins, C. C., Mechanical components of human eye movements, *J. Appl. Physiol.*, 26, 548, 1969.
15. Collins, C. C., The human oculomotor control system, in *Basic Mechanisms of Ocular Motility and Their Implications,* Lennerstrand, G. and Bach-Rita, P., Eds., Pergamon Press, New York, 1975, 145.
16. Collins, C. C., OMeara, D., and Scott, A. B., Muscle tension during unrestrained human eye movements, *J. Physiol.*, 245, 351, 1975.
17. Wilkie, D. R., *Muscle Studies in Biology,* Edward Arnold, London, 1968.
18. Levin A. and Wyman, J., The viscous elastic properties of a muscle, *Proc. R. Soc. London Ser. B.*, 101, 218, 1927.
19. Rack, P. M. H. and Westbury, D. R., The short range stiffness of active mammalian muscle and its effect on mechanical properties, *J. Physiol.*, 240, 331, 1974.
20. Hill, A. V., The series elastic component of muscle, *Proc. R. Soc. London Ser. B,* 137, 273, 1950.
21. Bahler, A. S., Modeling of mammalian skeletal muscle, *IEEE Trans. Biomed. Eng.*, BME-14, 249, 1968.
22. Scott, A. B., Strabismus — muscle forces and innervations, in *Basic Mechanisms of Ocular Motility and Their Clinical Implications,* Lennerstrand, G. and Bach-y-Rita, P., Eds., Pergamon Press, New York, 1975, 181.
23. Gordon, A. M., Huxley, A. F., and Julian, F. J., The variation in isometric tension with sarcomere length in vertibrate muscle fibers, *J. Physiol.*, 184, 170, 1966.
24. Goslow, G. E., Reinking, R. M., and Stuart, D. G., The cat step cycle: hind limb joint angles and muscle lengths during unrestrained locomotion, *J. Morphol.*, 141, 1, 1973.
25. Fenn, W. O. and Marsh, B. S., Muscular force at different speeds of shortening, *J. Physiol.*, 85, 277, 1935.
26. Hill, A. V., The heat of shortening and dynamic constraints of muscle, *Proc. R. Soc. London Ser. B,* 126, 136, 1938.
27. Katz, B., The relation between force and speed in muscular contraction, *J. Physiol.*, 46, 46, 1939.
28. Huxley, A. F., Muscle structure and theories of contraction, *Prog. Biophys. Biochem.*, 7, 255, 1957.
29. Joyce, G. C. and Rack, P. M. H., Isotonic lengthening and shortening movements of cat soleus muscle, *J. Physiol.*, 204, 475, 1969.
30. Joyce, G. G., Rack, P. M. H., and Westbury, D. R., The mechanical properties of cat soleus muscle during controlled lengthening and shortening movements, *J. Physiol.*, 204, 461, 1969.
31. Julian, F. J., The effect of calcium on the force-velocity relation of briefly glycerinated frog muscle fibers, *J. Physiol.*, 218, 117, 1971.
32. Julian, F. J. and Sollins, M. R., Regulation of force and speed of shortening in muscle contraction, *Cold Spring Harbor Symp. on Quant. Biol.*, 37, 635, 1973.

33. Partridge, L. D., Muscle properties: a problem for the motor physiologist, in *Posture and Movement: Prospective for Integrating Sensory and Motor Research on the Mammalian Nervous System,* Talbott, R. E. and Humphrey, D. R., Eds., Raven Press, New York, 1979, 189.

34. Clark, M. R., Jury, E. I., Krishnan, V. V., and Stark, L., Computer simulation of biological models using the inners approach, *Comput. Prog. Biomed.,* 5, 263, 1975.

35. Latimer, J. R., Troost, B. T., and Bahill, A. T., Linearization and sensitivity analysis of model for human eye movements, in *Modeling and Simulation, Proc. 9th Annu. Pittsburgh Conf.,* Vogt, W. and Mickle, M., Eds., Instrument Society of America, Pittsburgh, 1978, 365.

36. Stark, L., *Neurological Control Systems, Studies in Bioengineering,* Plenum Press, New York, 1968, 308.

37. Bahill, A. T., Latimer, J. R., and Troost, B. T., Linear homeomorphic model for human movement, *IEEE Trans., Biomed. Eng.,* BME-27, November 1980.

38. Lehman, S. and Stark, L., Simulation of linear and nonlinear eye movement models: sensitivity analyses and enumeration studies of time optimal control, *J. Cybern. Inf. Sci.,* 4, 1979.

39. Eykhoff, P., *System Identification — Parameter and State Estimation,* John Wiley & Sons, New York, 1974, chap. 2, 3, and 5.

40. Bekey, G. A. and Yamashiro, S. M., Parameter estimation in mathematical models of biological systems, *Adv. Biomed. Eng.,* 6, 1, 1976.

41. Latimer, J. R. and Bahill, A. T., Parameter estimation by function minimization using a modified steepest descent method, in *Modeling and Simulation, Proc. 10th Annu. Pittsburgh Conf.,* Vogt, W. and Mickle, M., Eds., Instrument Society of America, Pittsburgh, 1979, 683.

42. Bahill, A. T., Latimer, J. R., and Troost, B. T., Sensitivity analysis and validation of linear homeomorphic model for human movement, *IEEE Trans. Syst. Man Cybern.,* SMC-10, December 1980.

43. Taylor, S. R., Rudel, R., and Blinks, J. R., Calcium transients in amphibian muscle, *Fed. Proc. Fed. Am. Soc. Exp. Biol.,* 34, 1379, 1975.

44. Barmack, N. H., Bell, C. C., and Rence, B. G., Tension and rate of tension development during isometric responses of extraocular muscle, *J. Neurophysiol.,* 34, 1072, 1971.

45. Lennerstrand, G., Fast and slow units in extrinsic eye muscles of cat, *Acta Physiol. Scand.,* 86, 286, 1972.

46. Henneman, E., Peripheral mechanisms involved in the control of muscle, in *Medical Physiology,* Mountcastle, V. B., Ed., C. V. Mosby, St. Louis, 1974.

47. Burke, R. E., Rudemin, P., and Zajac, F. E., Catch property in single mammalian motor units, *Science,* 168, 122, 1970.

48. Sindermann, F., Geiselmann, B., and Fischler, M., Single motor unit activity in extraocular muscles in man during fixation and saccades, *Electroencephalogr. Clin. Neurophysiol.,* 45, 64, 1978.

49. Fuchs, A. F. and Luschei, E. S., Firing patterns of abducens neurons of alert monkeys in relationship to horizontal eye movement, *J. Neurophysiol.,* 33, 382, 1970.

50. Maeda, M., Shimazu, H., and Shinoda, Y., Inhibitory postsynaptic potentials in the abducens motoneurons associated with the quick relaxation phase of vestibular nystagmus, *Brain Res.,* 26, 420, 1971.

51. Baker, R. and Berthoz, A., Organization of vestibular nystagmus in oblique oculomotor systems, *J. Neurophysiol.,* 37, 195, 1974.

52. Keller, E. L., Participation of medial pontine reticular formation in eye movement generation in monkey, *J. Neurophysiol.,* 37, 316, 1974.

53. Evarts, E. V., Precentral and postcentral cortical activity in association with visual triggered movement, *J. Neurophysiol.,* 37, 373, 1974.

54. Abel, L. A., Dell Osso, L. F., and Daroff, R. B., Analog model for gaze-evoked nystagmus, *IEEE Trans. Biomed. Eng.,* BME-25, 71, 1978.

55. Zee, D. S. and Robinson, D. A., A hypothetical explanation of saccadic oscillations, *Ann. Neurol.,* 5, 405, 1979.

56. Robinson, D. A., Models of the saccadic eye movement control system, *Kybernetik,* 14, 71, 1973.

57. Thomas, J. G., The dynamics of small saccadic eye movements, *J. Physiol.,* 200, 109, 1969.

58. Childress, D. S. and Jones, R. W., Mechanics of horizontal movements of the human eye, *J. Physiol.,* 188, 273, 1967.

59. Reinhart, R. J. and Zuber, B. L., Parameters of the control signals for saccadic eye movement: electrical stimulation and modeling, *Exp. Neurol.,* 30, 148, 1971.

60. Zuber, B. L., Semmlow, J. L., and Stark, L., Frequency characteristics of the saccadic eye movement, *Biophys. J.,* 8, 1288, 1968.

61. Bahill, A. T., Clark, M. R., and Stark, L., Glissades — eye movements generated by mismatched components of the saccadic motoneuronal control signal, *Math. Biosci.,* 26, 303, 1975.

62. Bahill, A. T., Hsu, F. K., and Stark, L., Development, sensitivity analysis and predictions of a reciprocal innervation model for saccadic and vergence eye movements, in *Modeling and Simulation, Proc. 7th Annu. Pittsburgh Conf.,* Vogt, W. and Mickle, M., Eds., Instrument Society of America, Pittsburgh, 1976, 1245.

63. Selhorst, J. B., Stark, L., Ochs, A. L., and Hoyt, W. F., Disorders in cerebellar oculomotor control, *Brain,* 99, 497, 1976.

64. Zee, D. S. and Robinson, D. A., Clinical applications of oculomotor models, in *Topics in Neuro-opthalmology,* Thompson, H. S., Ed., Williams & Wilkins, Baltimore, 1979, 266.

65. Stark, L., Scott, A. B., and Kenyon, R. V., Dynamic overshoot in saccadic eye movements, *Soc. Neurosci.,* Abstr. 486, 1977.

66. Dell 'Osso, L. F., Robinson, D. A., and Daroff, B., Optokinetic asymmetry in internuclear ophthalmoplegia, *Arch. Neurol.,* 31, 138, 1974.

67. Kommerell, G., Internuclear ophthalmoplegia of aduction, *Arch. Opthalmol.,* 93, 531, 1975.

68. Fricker, J. and Sanders, J. J., Velocity and acceleration statistics of pseudorandomly timed saccades in humans, *Vision Res.,* 15, 225, 1975.

69. Metz, H., Saccadic velocity measurements in internuclear ophthalmoplegia, *Am. J. Ophthalmol.,* 81, 296, 1976.

70. Baloh, R. W., Yee, R. D., and Honrubia, V., Internuclear ophthalmoplegia, *Arch. Neurol.,* 35, 484, 1978.

71. Bahill, A. T., Hsu, F. K., and Stark, L., Glissadic overshoots are due to pulse width errors, *Arch. Neurol.,* 35, 138, 1978.

72. Bahill, A. T. and Stark, L., Overlapping saccades and glissades are produced by fatigue in the saccadic eye movement system, *Exp. Neurol.,* 48, 95, 1975.

73. Bahill, A. T. and Stark, L., The high-frequency burst of motoneuronal activity lasts about half the duration of saccadic eye movements, *Math. Biosci.,* 26, 319, 1975.

74. Holt, C. C., Modigliani, F., Muth, J. F., and Simon, H. A., *Planning Production, Inventories, and Work Force,* Prentice-Hall, Englewood Cliffs, N. J. 1960, 363.

75. Ford, A. and Gardiner, P. C., A new measure of sensitivity for social system simulation models, *IEEE Trans. Syst. Man Cybern.,* SMC-9, 105, 1979.

76. Frank, P. M., *Introduction to System Sensitivity Theory,* Academic Press, New York, 1978.

77. Melsa, J. L. and Jones, S. K., *Computer Programs for Computational Assistance in the Study of Linear Control Theory,* McGraw-Hill, New York, 1970.

78. Easter, S. S., A comment on the "glissade", *Vision Res.,* 13, 881, 1973.

79. Bahill, A. T. and Troost, B. T., Types of saccadic eye movements, *Neurology,* 29, 1150, 1979.

80. Bahill, A. T., Iandolo, M. J., and Troost, B. T., Smooth pursuit eye movements in response to unpredictable target waveforms, *Vision Res.,* 1980, in press.

81. Yasui, S. and Young, L., Preceived visual motion as effective stimulus to pursuit eye movement system, *Science,* 190, 906, 1975.

82. Young, L., Pursuit eye movements — what is being pursued?, in *Control of Gaze by Brain Stem Neurons,* Baker, R. and Berthoz, A., Eds., Elsevier/North-Holland, Amsterdam, 1977, 29.

83. Hsu, F. K., Krishnan, V. V., and Stark, L., Simulation of ocular dysmetria using a sampled-data model of the human saccadic system, *Ann. Biomed. Eng.,* 4, 321, 1976.

84. McDonald, J. D. and Bahill, A. T., Adaptive control model for the human smooth pursuit system, in *Modeling and Simulation, Proc. 11th Annu. Pittsburgh Conf.,* Vogt, W. and Mickle, M., Eds., Instrument Society of America, Pittsburgh, 1980.

85. Latimer, J. R. and Bahill, A. T., unpublished data.

SUBJECT INDEX — VOLUME 4

CRC Critical Reviews in Bioengineering

Page Numbers for Issues:

Issue 1, 1—112; Issue 2, 113 —201; Issue 3, 203—270; Issue 4, 271—355

AUTHOR INDEX — VOLUME 4

CRC Critical Reviews in Bioengineering

Page Numbers for Issues:

Issue 1, 1—112; Issue 2, 113—201; Issue 3, 203—270; Issue 4, 271—355